



OpenAIR@RGU

The Open Access Institutional Repository at Robert Gordon University

<http://openair.rgu.ac.uk>

This is an author produced version of a paper published in

Wear (ISSN 0043-1648)

This version may not include final proof corrections and does not include published layout or pagination.

Citation Details

Citation for the version of the work held in 'OpenAIR@RGU':

AHMED, R., ALI, O., FAISAL, N. H., AL-ANAZI, N. M., AL-MUTAIRI, S., TOMA, F.-L., BERGER, L.-M., POTTHOFF, A. and GOOSEN, M. F. A., 2015. Sliding Wear Investigation of Suspension Sprayed WC-Co Nanocomposite Coatings. Available from *OpenAIR@RGU*. [online]. Available from: <http://openair.rgu.ac.uk>

Citation for the publisher's version:

AHMED, R., ALI, O., FAISAL, N. H., AL-ANAZI, N. M., AL-MUTAIRI, S., TOMA, F.-L., BERGER, L.-M., POTTHOFF, A. and GOOSEN, M. F. A., 2015. Sliding Wear Investigation of Suspension Sprayed WC-Co Nanocomposite Coatings. *Wear*, 322-323, pp. 133–150.



This work is licensed under a Creative Commons Attribution - Non-Commercial - No-Derivatives 4.0 International Licence

Copyright

Items in 'OpenAIR@RGU', Robert Gordon University Open Access Institutional Repository, are protected by copyright and intellectual property law. If you believe that any material held in 'OpenAIR@RGU' infringes copyright, please contact openair-help@rgu.ac.uk with details. The item will be removed from the repository while the claim is investigated.

NOTICE: this is the author's version of a work that was accepted for publication in *Wear*. Changes resulting from the publishing process, such as peer review, editing, corrections, structural formatting, and other quality control mechanisms may not be reflected in this document. Changes may have been made to this work since it was submitted for publication. A definitive version was subsequently published in *WEAR*, [VOL 322-323, 2015]
DOI <http://dx.doi.org/10.1016/j.wear.2014.10.021>

Please note that the illustrative material which accompanied this text is provided in a separate file.

Sliding Wear Investigation of Suspension Sprayed WC-Co Nanocomposite Coatings

R. Ahmed^{a,b1}, **O. Ali**^b, **N. H. Faisal**^{a,c}, **N. M. Al-Anazi**^d, **S. Al-Mutairi**^d, **F.-L. Toma**^e, **L.-M. Berger**^f, **A. Potthoff**^f, **M. F. A. Goosen**^g

^a College of Engineering, Alfaisal University, P.O. Box 50927, Riyadh, 11533, Saudi Arabia

^b School of Engineering and Physical Sciences, Heriot-Watt University, Edinburgh, EH14 4AS, UK

^c School of Engineering, Robert Gordon University, Garthdee Road, Aberdeen, AB10 7GJ, UK

^d Materials Performance Unit, Research & Development Centre, Saudi Aramco, Dhahran, 31311, Saudi Arabia

^e Fraunhofer Institute for Material and Beam Technology - IWS, Winterbergstrasse 28, D-01277 Dresden, Germany

^f Fraunhofer Institute for Ceramic Technologies and Systems - IKTS, Winterbergstrasse 28, D-01277 Dresden, Germany

^g Office of Research & Graduate Studies, Alfaisal University, P.O. Box 50927, Riyadh 11533, Saudi Arabia

ABSTRACT

Sliding wear evaluation of nanostructured coatings deposited by Suspension High Velocity Oxy-Fuel (S-HVOF) and conventional HVOF (Jet Kote (HVOF-JK) and JP5000 (HVOF-JP)) spraying were evaluated. S-HVOF coatings were nanostructured and deposited via an aqueous based suspension of the WC-Co powder, using modified HVOF (TopGun) spraying. Microstructural evaluations of these hardmetal coatings included X-ray Diffraction (XRD) and Scanning Electron Microscopy (SEM) equipped with Energy Dispersive X-ray Spectroscopy (EDX). Sliding wear tests on coatings were conducted using a ball-on-flat test rig against steel, silicon nitride (Si₃N₄) ceramic and WC-6Co balls. Results indicated that nanosized particles inherited from the starting powder in S-HVOF spraying were retained in the resulting coatings. Significant changes in the chemical and phase composition were observed in the S-HVOF coatings. Despite decarburization, the hardness and sliding wear resistance of the S-HVOF coatings was comparable to the HVOF-JK and HVOF-JP coatings. The sliding wear performance was dependent on the ball-coating test couple. In general a higher ball wear rate was observed with lower coating wear rate. Comparison of the total (ball and coating) wear rate indicated that for steel and ceramic balls, HVOF-JP coatings performed the best followed by the S-HVOF and HVOF-JK coatings. For the WC-Co ball tests, average performance of S-HVOF was better than that of HVOF-JK and HVOF-JP coatings. Changes in sliding wear

¹ Corresponding author R.Ahmed@hw.ac.uk

behavior were attributed to the support of metal matrix due to relatively higher tungsten, and uniform distribution of nanoparticles in the S-HVOF coating microstructure. The presence of tribofilm was also observed for all test couples.

Keywords: Nanostructured coating, sliding wear, WC-Co coating, suspension spraying, tribology.

1. INTRODUCTION

Hardmetals, such as WC-Co, Cr₃C₂-NiCr, WC-(W,Cr)₂C-Ni, WC-NiCrBSi belong to one of the most important group of materials processed by thermal spray processes into coatings, which are predominantly applied for the protection against wear, such as abrasion, erosion and sliding [1-13]. Third generation high velocity oxy-fuel spraying (HVOF) is currently the industrial state-of-the-art process for the preparation of high quality hardmetal coatings. Tribomechanical properties such as hardness, wear resistance, and strength are influenced primarily by the size and distribution of WC grains, the porosity, the volume fraction and thermo-mechanical properties of the metal matrix, and post-treatments of the composite hardmetal coating [1-6, 14-22]. Both room temperature and higher temperature investigations have been conducted [23-26]. These coatings are used in many industrial applications ranging from aerospace, transportation, off-shore and civil engineering to biomedical industries. During spraying of WC-Co powders, significant changes in the chemical and phase compositions can occur [8]. He and Schoenung [27] indicated the potential benefits of nanostructured WC-Co coatings over conventional WC-Co coatings. However in the past, coatings deposited from nanostructured powders often displayed a much less real gain in coating properties than expected, e.g. WC-Co coatings usually showed higher hardness but lower wear resistance than conventional coatings and thus a disappointing performance [28].

The past two decades have seen extensive research in optimizing the feedstock powder characteristics, process parameters, and post-treatments of wear resistant hardmetal coatings [1-6, 12, 14-19]. Most research however has related to coatings sprayed from agglomerated and sintered powders, with the average particle size ranging from 10 μm to 50 μm and WC grain size ranging from 0.8 to 3.5 μm [1-6]. Optimization of these coatings has resulted in coating microstructures with negligible porosity, high fracture toughness and minimization of secondary carbide phases [1-6, 9-16].

Nanostructured feedstock powders cannot be directly fed into spray processes, e.g. the initial hardmetal constituents can firstly be agglomerated into spherical particles with μm-particle sizes for spraying. Many researchers have used conventional thermal spray systems to deposit coatings from

nanostructured WC-Co feedstocks [14-15, 29-31]. In these previous investigations, the problems associated with the injection of submicron particles have been addressed via agglomeration of nanoparticles to micron sized powder for thermal spraying [14-15, 29-31]. For conventional spraying systems, the use of agglomerated nanosized particles for nanostructured thermal spray coatings can result in a predominantly bimodal coating structure where the coating architecture exhibits micrometer-sized zones with nanometer-sized structure [29].

Suspensions are an emerging type of feedstock for thermal spray processes, which allows the direct injection of very fine powders (from nm- up to several μm -sizes), thus avoiding the necessity of powder agglomeration [29,30,32]. Using suspensions, finely structured coatings can be produced, but their use is limited so far to oxide materials [33-35]. Mostly water [29, 13, 36-37] and alcohols e.g. isopropanol and ethanol [29, 38], have been employed as transport media to inject fine nanosized and submicron-sized particles directly into the thermal spray process. Suspension sprayed coatings, because of the relatively smaller powder particle size, also result in lower as-sprayed surface roughness and additionally provide the ability to deposit thinner thermal spray coatings [33-34]. Apart from powder particle size, other differences also occur in terms of particle temperature and velocity e.g. between HVOF and APS systems adapted for suspension spraying.

Suspension spraying can result in either a truly nanocomposite coating, or a bimodal coating i.e. a lamellar coating with nanostructured zones [29]. The microstructure features of the suspension sprayed coatings are not only strongly depended to the suspensions characteristics (i.e. particle sizes, agglomeration degree of very fine nano-sized particles, stability, and viscosity) but also the spray processes and parameters. The bimodal coating in suspension spraying results from the thermal kinetics of nanosized particles which agglomerated during preparation in suspension. These agglomerates/aggregates cannot be completely de-agglomerated (up to nano-size as primary particle size) during spraying. During cold spraying, these agglomerated nanoparticle zones may be observed in the coating microstructure. When spraying with “hot” parameters, these regions are less evident because the agglomerates are completely or mostly melted resulting in splats of several μm .

Even for oxides, there are only few studies on the dry sliding wear resistance of coatings sprayed from suspensions. Some results have been reported for Al_2O_3 and TiO_2 coatings against sintered alumina [39-40]. However, these coatings were produced from suspensions with low solids content, thus representing uneconomic conditions for coating deposition compared to conventional coatings.

In the case of conventional HVOF-sprayed hardmetal coatings all metal binder areas are nanostructured due to rapid solidification of powder particles, however their concentration can be increased by the use of suspensions of nanocomposite powders. In the literature, there is only one study by Oberste Berghaus et al. [32], dealing with the preparation of WC-12Co coatings by plasma spraying using suspensions. They have used a mixture of ethanol and ethylene glycol for suspension preparation and studied coating microstructure and phase composition in detail, but no experiments of wear properties were reported.

The dry sliding wear resistance of a new generation suspension thermal spray WC-Co coatings has not been reported in the published literature. Prior studies on the effect of grain size on the sliding wear resistance have shown wear rates which are very dependent on the tribological test conditions, e.g. it has generally been reported that the wear resistance of thermally sprayed WC-Co coatings increases with a decrease in the volume fraction of Co, and increases dramatically as the WC grain size is reduced [1-6]. Contrary to this, it has also been reported that the wear rate increases with the increasing carbide grain size, as the finer carbides in the wear debris relatively reduce the three-body abrasion wear process [2]. Similarly, the results are dependent on the counter-body (ball or pin) material, which makes the comparison of wear rates and failure mechanisms for different test couples difficult.

Previously, the authors reported investigations of another nanostructured WC-12Co coating deposited by S-HVOF spraying using suspension made from milled agglomerated and sintered conventional powder [41]. As it is advantageous to avoid milling operations, in this paper, a WC-12Co nanocomposite powder was employed. The current paper which aims to address some of these issues, has three specific objectives *i)* investigate the sliding wear resistance of a

nanocomposite WC-Co coating deposited by suspension thermal spraying, *ii*) comparison of sliding wear performance of suspension sprayed coatings with first (Jet Kote) and third generation (JP5000) conventional HVOF coatings, and *iii*) influence of counter-body as steel, ceramic and sintered carbide on the relative sliding wear performance under test conditions similar to ASTM G133-02. Tribo-mechanical investigations included Scanning Electron Microscopy (SEM), Energy Dispersive X-ray Spectroscopy (EDX), X-Ray Diffractometry (XRD), nanohardness and sliding wear evaluations.

2. TECHNOLOGICAL CHALLENGES – Suspension spraying of WC-Co coatings

There are seven major technological challenges associated with the direct use of nanoparticles such as WC-Co in thermal spraying systems [29-30, 32], which have so far limited the development of WC-Co nanocomposite coatings by spraying with suspensions for industrial applications. The first four can be overcome by the use suspension thermal spraying, whereas the remaining three require careful considerations of suspension composition [41].

- i.* Direct injection of nanoparticles in thermal spray process cannot be done using conventional conditions due to their lower mass relative to conventional powders.
- ii.* Even if the nanoparticles are injected, they can decompose quickly owing to the high thermal energy imparted as a result of their smaller size.
- iii.* The atmosphere of thermal spraying can lead to carbon loss in high temperature environments, which can increase due to the small grain size of WC compared to conventional feedstocks.
- iv.* There is generally an uneven distribution of nanocomposite particles in the spray stream. These challenges can however be somewhat addressed by employing a suspension feed system and carefully controlling the coating process parameters.
- v.* Suspension development and its feed-mechanism need to be optimized before improved coating quality can be achieved i.e. the high density of WC (15.7 g/cm^3) makes suspension development difficult in comparison to other carbides as it is almost three times the density of TiC (4.93 g/cm^3) and more than twice that of Cr_3C_2 (6.68 g/cm^3).

- vi. WC-Co can pose specific problems in aqueous suspension as oxides existing at the surface of WC are acidic and that of Co (CoO) are basic in nature [25-26]. This difference in the acidic and alkaline nature can however be avoided by employing a preformed WC-Co composite powder.
- vii. In aqueous suspensions Co can dissolve which influences the stability of the suspension. Suspensions containing these nanoparticles therefore pose complex chemical interactions leading to agglomeration and/or segregation, that could be difficult to control while maintaining the required pH level.

One second generation HVOF spray gun has been adopted for the use of suspensions, allowing axial injection directly into the burning chamber. This development has been combined with the development of water-based suspensions with high solids content. The vaporization of water and the resulting cooling effect might be also advantageous for WC-Co coatings. On the other hand the water vapor is a strong oxidizing agent during spraying, but is already present in all HVOF processes due to fuel combustion [38].

In conventional spray processes the surrounding oxygen still provides an additional oxidising environment to the powder particles. Only further investigations in this area can clarify the outcome of these two competing processes of cooling and oxidizing environments. The coating process parameters likewise need to be further optimized for the nanocomposite coatings as the powder particle size and its feed mechanism are different from conventional thermal spray coatings.

3. EXPERIMENTAL

3.1 Coating Deposition

For S-HVOF spraying, a nanosized WC-12wt.%Co powder (200 nm WC grain size, Dong Yang (HK) Int'l group Limited, China) was used to produce the aqueous suspensions. According to the powder manufacturer the powder consisted of fine nano- and submicron-sized particles, however the powder showed a strong tendency to agglomerate. Consequently the particles could not be employed as-received to produce the suspension, but a milling process performed in a planetary ball

mill was necessary to decrease the size distribution of the particles in the powder for S-HVOF spraying.

After milling, the powders were characterized for particle size (Table 1) using a Mastersizer 2000 apparatus (Malvern Instruments Ltd.). The measurement characterized the particle size distribution of the powders by laser diffraction in the measuring range between 20 nm and 2000 μm . All analysis was conducted in dilute suspension. Prior to analysis the powder was dispersed in liquid by energy input (ultrasound). Sample preparation for powder analysis and measurement itself were done according to ISO14887:2000 and ISO13320:2009. The size distribution was calculated from the raw data by Mie theory with a refractive index of 3.5.

The suspensions were produced by dispersion of 25 wt.% milled powder in deionized water. About 1 wt.% (referring to the solid content) of an organic dispersant (polyethylenimine) was added to improve the homogeneity and stability of suspension. S-HVOF spraying was conducted using a modified HVOF (TopGun, GTV mbH, Luckenbach, Germany) spray process using ethylene as fuel gas [33-35, 42]. Four different S-HVOF spray parameter sets were employed (labeled as conditions #1 to #4 in Table 2). The process parameters were varied in order to achieve long-term stability of the spray process to deposit coatings with low porosity.

In order to compare the performance of nanocomposite S-HVOF coatings with conventional coatings, HVOF-JK (Jet Kote) and HVOF-JP (JP5000-Table 3) coatings by means of a WC-12wt.% Co agglomerated and sintered powders were prepared. Industrially optimized coating process parameters were used for these conventional HVOF coatings. The fracture response of the HVOF-JK coatings has previously been reported by the authors [43]. HVOF-JK is a first generation HVOF spray gun which is gas-fuelled. HVOF-JP is a more advanced third generation liquid-fuelled HVOF system. Further details of these HVOF systems are described elsewhere [44].

All coatings were deposited on AISI440C steel discs of 31 mm diameter and 6 mm thickness. Substrate material for all coatings was grit blasted prior to the coating deposition. The surface of as-

deposited coatings was ground and polished prior to tribological wear testing. The coating thickness and average of five hardness values of all coatings are shown in Table 4.

3.2 Microstructural Evaluations

The microstructure of the powders and coatings was observed via scanning electron microscopy (SEM) by secondary electron (SE) and backscattered electron (BE) imaging equipped with energy dispersive x-ray spectroscopy (EDX). Observations were made on the polished cross-sections. The compositions of microstructural phases in the powders and coatings were determined via X-ray diffraction (XRD) with Cu-K α radiation (wavelength = 1.5406Å).

In order to ascertain the changes in the chemical and phase compositions due to thermal load in the spray process, coating segments detached from the substrate were analyzed for their total carbon content by the combustion method (CS 230, LECO Corporation, St. Joseph, MI, USA) and oxygen content by the carrier gas hot extraction (TCH 600, LECO Corporation, St. Joseph, MI, USA). Suspension coatings were also heat treated (Hot Isostatically pressed (HIPed) at 920 °C for 2 hours at 103MPa in an inert atmosphere) for investigation of transformation of the amorphous constituents into a crystalline state.

3.3 Sliding Wear Investigations

The sliding wear resistance was examined via ball-on-flat tests. These tests were conducted unlubricated at room temperature on a bench mounted wear test machine (BLR2000M; Bud Labs, USA). The ball-on-flat tests were conducted using three different ball materials i) AISI 440C steel ball (12.7mm diameter), ii) Si₃N₄ ceramic ball (12.7mm diameter) and iii) Sintered WC-6%Co ball (9.5mm diameter) against the coated disc sample under a normal load of 25 N for all counterparts. The test conditions were similar to ASTM G133-02 (procedure A), except that the ball radius varied slightly. Sliding wear tests were conducted for a sliding distance of 500 m. The average surface roughness (R_a) of the disc samples was 0.05 μ m. During the test, the disc experienced reciprocating sliding motion at an oscillating frequency of 2.0 Hz, with a stroke length of 10 mm. Five tests were conducted for each test couple. Wear volume loss of the coating was computed from the length of

the stroke and the average cross-sectional area of the wear grooves, which was measured via the interferometer (Zygo New View). The corresponding ball volume loss was calculated using the following geometrical relation:

$$V = \frac{\pi H^2}{3}(3R - H), \quad \text{Eq.1}$$

where $H = R - \sqrt{R^2 - r^2}$ and “ R ”, “ r ” are the ball radius and ball-wear-scar radius, respectively. This methodology is consistent with the ball volume loss calculations adapted in ASTM G99 and ASTM G133-02. The wear scars and debris after the sliding wear tests were examined by optical and scanning electron microscopy. The friction coefficient was evaluated using a tension-compression load cell mounted on the sliding wear rig. Averaged friction coefficient values and their standard deviation are presented in the results section.

4. RESULTS

4.1 Microstructural Characterization

Figure 1a shows the SEM micrograph of the as-received nanosized WC-Co powder. Due to the agglomeration of the powder, the nanosized behavior of the as-received powder could not be confirmed. The powder contained μm -sized particles showing an inhomogeneous morphology with a very wide range of particle sizes and irregular shapes: spherical particles with sizes up 200-300 nm; sub-micro-sized sintered aggregates with elongated shape and micro-sized compacted sintered particles with irregular surface. The measurement of the particle size distribution and the very low value of the specific surface area of about $0.9 \text{ m}^2/\text{g}$ (calculated from 5 points of the nitrogen adsorption isotherm by using the BET model) confirmed also the SEM observations. As summarized in Table 1, the particle sizes of as received powder varied from $1.95 \mu\text{m}$ ($x_{10;3}$) to $21.5 \mu\text{m}$ ($x_{90;3}$) with an average particles size of about $9.1 \mu\text{m}$ ($x_{50;3}$). Because of the presence of coarse particles and the high tendency of aggregation of the powder, milling was necessary to reduce the particle size. The particles sizes of the milled powder (Figure 1b) was reduced to $x_{10;3} = 0.49 \mu\text{m}$, $x_{50;3} = 1.35 \mu\text{m}$ and $x_{90;3} = 4.6 \mu\text{m}$ (Table 1). Moreover, the nanosized behavior of the milled powder was confirmed by the high value of the specific surface area of about $20 \text{ m}^2/\text{g}$. The aqueous suspension produced from the milled powder showed a low viscosity and a Newtonian behavior.

Figure 2 shows the SEM observations of S-HVOF coatings substrate system related to deposition conditions #1 to #4 (Table 2). The S-HVOF coatings are dense structured and well bonded to the substrate. Some internal cracking due to high thermal stresses could be observed for samples S-HVOF#2. Higher magnification cross-section SEM images of these coatings are shown in Figure 3. At higher magnification, the suspension sprayed coatings showed a specific microstructure (lamellar-like) with fine submicron-sized particles; the presence of micron-sized pores was observed. Figure 4 displays the SEM results of the cross-sections of the HVOF-JK and HVOF-JP coatings. The XRD of milled powder and as-deposited S-HVOF coatings are shown in Figure 5, whereas Figure 6 demonstrates the XRD diffraction patterns of the conventional HVOF-JK and HVOF-JP coatings. The XRD diffraction patterns of S-HVOF deposition conditions # 3 and # 4 were similar to that of # 1 and #2 and are not shown in Figure 5. In order to investigate the changes of chemical and phase compositions in more detail, the S-HVOF coatings under deposition condition # 4 were also heat-treated using inert atmosphere in a HIPing (Hot Isostatic Pressing) vessel at 920 °C for 2 hours at a pressure of 103MPa. The XRD diffraction pattern of this heat-treated coating is also revealed in Figure 5 to aid the discussion.

The XRD pattern of both S-HVOF coatings show amorphous/nanocrystalline “humps”, with a position of the maximum corresponding to metallic tungsten. Peaks of WC and W₂C were also present, the latter with a shift compared to the standard. The non-metal analysis indicated that for the coating deposited under condition # 2, the carbon and oxygen content was 2.0% and 1.8%, respectively.

The hardness measurements (Table 4) for suspension sprayed coatings showed values between 890 and 940 HV0.3 with a highest value for S-HVOF#4 (with exception of the sample S-HVOF#3 where because of the low coating thickness only a representative value is given), which was comparable to HVOF-JK, but slightly lower than HVOF-JP values. A notable result was the relatively lower standard deviation of hardness for the suspension sprayed coatings compared to the coatings produced from powders.

4.2 Sliding Wear Tests

In the case of S-HVOF coatings the sliding wear tests were conducted for the deposition condition S-HVOF#4, due to its high hardness. S-HVOF coatings deposited under deposition condition # 4 provided a stable and continuous coating spray process to manufacture thick coatings of about 200 μm without the problems of internal cracking (Figure 2b). This deposition condition also provided the highest average microhardness. Figure 7 illustrates the SEM observations of the wear track for S-HVOF coatings which slid against the steel ball. Figure 8 shows the SEM observations of test couples which involved WC-Co ball. Representative SEM observations of the S-HVOF coating and ceramic ball test couples are revealed in Figure 9. The average values of wear rate recorded after the sliding wear tests are displayed in Figures 10. These values (including the standard deviations) are presented as the ball volume loss, coating wear rate and total wear rate, respectively. Average friction coefficient values recorded during the sliding wear tests are shown in Figure 11. The standard deviation of these averaged friction values are also indicated in Figure 11. The SEM observations of the ball surface after the sliding wear tests are displayed in Figure 12, whereas Figure 13 shows the SEM observation of the wear debris after the sliding wear tests.

5. DISCUSSION

5.1 Coating Microstructure

The cross-sections of the suspension sprayed hardmetal coatings revealed in Figures 2 and 3 presents fully molten splats, indicating thorough heating of the coating particles. The lamellar-like structure observed in Figure 3 is also consistent with good wettability and flattening of powder particles on impact. Comparisons of SEM observations shown in Figures 3 indicate nanocomposite features that are consistent with the milled powder particle distribution (as shown in Table 1). Higher magnification inserts in Figure 3c,d indicate the approximate size of some the nanocomposite features. Despite the carbon loss, these nanostructured features were well distributed within the microstructure, indicating uniform distribution of the powder particles in the S-HVOF spray system. At the coating / substrate interface, the coating follows the profile of grit-blasted substrate with negligible porosity. This is typical of HVOF coatings that impart relatively higher

particle velocity, providing a peening effect in comparison to the plasma spray processes. The presence of tiny pores and interlamellar oxides can also be observed in Figure 3.

One of the main problems associated with suspension spraying is the long-term stability of the coating process, as clogging of the spray gun (spitting) can occur [45]. Optimisation of suspension and coating process parameters for hardmetals such as WC-Co is significantly more difficult as indicated in section 2. A number of variants of spray conditions and suspension concentrations were therefore attempted, but only the results of four conditions are indicated here (Table 2). The stability of the coating process is also dependent on the solid content e.g. as the solid content increases, the water content to vaporise per unit volume of the slurry feed rate is lower, this imparts more heat on the powder particles and result in non-uniform heating of powder. The solid content in the current investigation was kept at 25%, which was based on a previous investigation [41]. It was possible to achieve a coating thickness in excess of 100 μm for all deposition conditions as demonstrated in Table 2, but the S-HVOF deposition condition # 4 provided the best combination of coating thickness, process stability and microhardness (Tables 2 and 4). The internal stresses after spraying with deposition condition # 2 led to cracks for thicker coatings (Figure 2b).

Comparison of S-HVOF coatings observed in Figure 3 with conventional HVOF coatings shown in Figure 4 indicates distinctive features. The carbide grain size, which is typically around 3 μm to 5 μm in Figure 4, is well preserved and distributed in the deposited coating, and is larger than the sub-micron carbide size seen in Figures 3. The microstructural observations of the HVOF coatings shown in Figure 4 are consistent with published literature [1-6].

The XRD comparison of milled powder and deposited coatings provide further insights into the deposition processes during S-HVOF and conventional HVOF spraying. A comparison of the XRD pattern of the conventional HVOF coating (Figure 6) indicate sharp WC peaks that are well retained in the coating. This suggests that HVOF process parameters were optimized leading to only a small decarburization, resulting in a low amount of detectable W_2C . In contrast, the XRD patterns of the S-HVOF coatings (Figure 5) indicate some retained WC, W with some W_2C shifted peak positions,

but the pattern is dominated by a “nanocrystalline peak” between 2θ values of 35 to 48 degrees. The presence of nanocrystals in this S-HVOF WC-Co coatings was similar to a recently reported transmission electron microscopy investigation for another coating [41]. The XRD-analysis of the powder showed that besides WC and Co phases, W_2C and traces of eta-phases (Co_3W_3C , Co_6W_6C) were also present (Figure 5). For discussion purpose, these nanocomposite particles in the deposited S-HVOF coating will be collectively termed as “nanosized particles”. These nanosized particles were well distributed within the microstructure, indicating uniform spray conditions for the powder particles in the S-HVOF spray process. Comparison of Figures 5 and 6 shows that the S-HVOF deposition process led to intensive structural changes in the material. The XRD patterns of the milled spray powder demonstrates mainly tungsten carbide (WC) peaks which also indicate that the decarburisation occurred during the S-HVOF coating deposition process. A comparison with the XRD pattern presented by Oberste Berghaus et al. [32] shows, that the height of the amorphous/nanocrystalline “hump” is more intensive compared to those of WC. No metallic Co was observed in the S-HVOF or HVOF coatings suggesting that it became part of the amorphous/nanocrystalline matrix. Therefore, an amorphous or nanocrystalline binder phase was produced as observed in Figure 5. In addition, the XRD diffraction pattern of suspension sprayed WC-12Co in this work resembles those of Detonation Gun Spray (DGS) coatings, sprayed with excess of oxygen [13].

The carbon analysis of the coating indicates carbon loss which was higher than expected (carbon: 2.0%). At the same time the oxygen content (oxygen 1.8%) is also higher than usually observed for WC-Co coatings (typically < 0.2 wt. % [8]). This is a higher carbon content, but also a higher oxygen content than measured recently for a suspension sprayed coating from another powder [41]. Both W_2C and metallic tungsten are often detected in the as-sprayed WC-Co coatings [46], including earlier studies of Verdon et al. [47] and Stewart et al. [48]. Both studies [47,48] investigated the formation of WC-Co coatings with HVOF spray processes which were identical or comparable with the spray process in the current study, using conventional and nanostructured agglomerated and sintered feedstock powders. Stewart et al. [48] have shown that the formation of metallic tungsten depends on the carbide grain size. Thus the higher carbon loss observed in the

current study is in agreement with the results of Stewart et al. [48] taking into account the feedstock properties and spray conditions. Both studies also proposed mechanisms of W_2C and metallic tungsten formation, which are however different and indicate the need of further research, considering also the results of the current study.

Heat treatment of WC-Co in an inert atmosphere above 600 °C can lead to structural changes, bringing the phase composition closer to the equilibrium state, as discussed earlier [8, 46]. The M_6C (Co_3W_3C) and $M_{12}C$ (Co_6W_6C), the so-called η -phases, are possible equilibrium phases in the W-C-Co system, after loss of carbon in the spray process. Sometimes, their existence in as-sprayed coatings is also reported, as summarized in earlier studies [8, 46]. After the heat treatment at 920 °C WC, metallic tungsten and two η -phases M_6C (Co_2W_4C fit the peaks better than those of Co_3W_3C) and $M_{12}C$ (Co_6W_6C) were observed in the coating. This phase composition confirms the strong carbon loss. However, it should be mentioned that as a result of the heat treatment, a decrease both of the carbon and oxygen contents is possible, due to internal reduction processes. Previous research by the investigators has shown that heat-treatment of HVOF WC-Co and WC-NiCrBSi coatings can be effectively employed to crystallize amorphous phases and hence further improve the tribomechanical performance of coatings [8-11, 20-22, 46]. This can be also applicable to S-HVOF coatings.

According to the W-C phase diagram [49], W_2C is thermodynamically unstable. Below 1250 °C it can decompose into WC and W during cooling of the WC-Co particle after impact. This decomposition can also result from the heat treatment at 920 °C. Annealing of the coating where Co is present will form the eta-phases as mentioned above, and Co can be fully consumed by these reactions. However, any nanoparticles appearing in the as-sprayed coating will strengthen the binder phase and can alter the tribological wear mechanism. Additional studies are needed however to fully understand the microstructure of these nanocomposite hardmetal coatings.

In general, dense coatings containing nanosized particles were achieved for all S-HVOF deposition conditions considered in this investigation. The microstructure and phase composition of HVOF-JK

and HVOF-JP coatings was consistent with low decarburization associated with these coatings in the published literature. The microhardness of S-HVOF coatings was comparable to the HVOF-JK coatings. Both S-HVOF and HVOF-JK coatings showed slightly lower microhardness in comparison to the third generation HVOF-JP coatings (Table 4). The influence of differences in these microstructural phase, carbide size, and hardness on the wear resistance of HVOF coatings is discussed in the next section.

5.2 Sliding Wear Analysis

The total wear rate (or volume loss) for the sliding wear test was dependent on the ball-coating test couples. In general a higher wear rate for the ball material was observed with a lower coating wear rate (Figure 10). Comparison of total wear rate (ball and coating) indicated that for steel ball test couples, HVOF-JP coatings performed the best followed by the S-HVOF and HVOF-JK coatings. For the Si₃N₄ ceramic ball test couples, average performance of HVOF-JP was better, followed by the HVOF-JK and S-HVOF coatings. For the WC ball tests, the average performance of S-HVOF coatings was better than that of HVOF-JK and HVOF-JP coatings (Figure 10c). The main difference between the test couples originated from the ball wear rate (Figure 10a). This is attributed to the presence of carbides in wear debris, which influenced the three-body abrasive wear process.

5.2.1 Comparison between S-HVOF, HVOF-JK and HVOF-JP coatings against steel balls

Considering the higher hardness of the HVOF coatings (Table 4) in comparison to the steel ball ($HV_{0.3} \approx 400$), the ball wear loss is expected to be the highest for the steel ball test couples considered in this investigation (Figure 10a). The fracture toughness (K_{IC}) of HVOF-JK and HVOF-JP coatings was previously reported as $5.2 \pm 0.5 \text{ MPa m}^{1/2}$ and $7.4 \pm 0.5 \text{ MPa m}^{1/2}$, respectively [50]. Fracture toughness was not measured for the S-HVOF coatings, however considering the carbon loss and eta-phase formation discussed earlier, a lower conservative value of $3 \text{ MPa m}^{1/2}$ was assumed for further analysis [50]. The fracture toughness of the steel ball was much higher ($\approx 95 \text{ MPa m}^{1/2}$). Given the high fracture toughness of the steel ball, the ball wear mechanism was expected to be dominated by the plastic deformation in two and three-body abrasion.

Rajinikanth et al. [3] recently reported a pin-on-disc (ASTM G99-05) investigation of WC-Co coated discs sliding against the steel pins. They indicated that in the test couples involving WC-Co coating against the steel counterface, the wear process starts with a transfer film resulting in a negative wear at the start of the test. Engqvist et al. [5] has indicated the origin of the tribofilm in air and nitrogen environments and showed that in mild test conditions, cemented WC-Co carbides result in thick tribofilm (a couple of μm thick) with low amounts of oxides. They also pointed out that at more severe test conditions the tribofilm became thinner ($< 1\mu\text{m}$) and contained large amounts of oxides, together with WC and Co. A similar mechanism of transfer film was observed against the steel balls as shown in Figure 7d where the oxygen content was negligible and the Fe from the ball surface transferred to the coating surface. This is consistent with previous investigation and represents the start of the wear process in the form of Fe transfer film with negligible oxide content [3,5]. An oxygen content of $\approx 20\%$ to 30% was also observed on the parts of the wear track surface (Figure 8c), which represents the role of oxygen due to flash temperature at the asperity contact. EDX map for oxygen in Figure 8e further confirms the role of oxygen in steady state wear process. Wear debris (Figure 13a), also indicated a highly oxidized transfer film during the sliding wear test conditions. This was indicative of all coating test couples which involved the steel ball. Apart from the dominant role of the transfer film, the two and three-body abrasion mechanism modified the wear rate behavior of the S-HVOF, HVOF-JK and HVOF-JP coatings.

Yang et al. [2] reported the effect of grain size on the microstructure and sliding wear behavior of HVOF sprayed WC-Co coatings. They indicated that for the WC grain size range of 0.8 to $2.8\ \mu\text{m}$, the coating wear rate increased with the increasing carbide size. They related this to the wear mechanism which was dominated by the binder extrusion, followed by the carbide pull-out and fracture. The presence of the tribofilm was also reported, which is consistent with the observations in the current investigation. They concluded that as the carbide size in the wear debris decreases, the severity of damage to the coating and counterbody also decreases in comparison to the larger carbide size coating, which resulted in a lower wear rate with decreasing carbide size.

Comparison of the S-HVOF and HVOF-JK coatings in the current investigation indicated a similar trend of ball wear (Figure 10). The case is however different for the HVOF-JP coatings, which showed an opposite trend due to the changes in the wear mechanism. This dependency of wear rate on the failure mechanism is consistent with the studies reported by Shipway et al. [1]. They concluded that the finer carbide nanostructured coatings had relatively higher wear rate, as the wear mechanism was fracture dominated, which was caused by the loss of ductility in the binder phase due to the decomposition of WC grains during spraying. Although in the current investigation decarburization of the coating was observed, which should reduce the binder ductility, however the fracture of the S-HVOF coatings was not observed under the tribological conditions adapted in this investigation. There was also a difference in the fracture failure mode of the coating when comparing the ductility of cobalt matrix as indicated by Shipway et al. [1], and the strength of the bond between the cobalt binder and WC phase as highlighted by Wood [4]. This can be further considered on the basis of the earlier discussion in section 5.1, which indicated that the heat-treatment of WC-Co hardmetal results in the formation of M_6C and $M_{12}C$ phases (eta-phases). These phases are expected to be brittle and their formation continues, as long as the temperature and environmental conditions favor their development, until the entire cobalt is consumed in the process. The loss of cobalt will therefore result in loss of ductility. However previous investigations by the authors have concluded that the formation of eta-phases after the heat-treatment of WC-Co coatings results in higher fracture toughness, elastic modulus and wear (sliding wear and contact fatigue) resistance [9-11, 19-22, 43, 50]. The only difference in the morphology of these eta-phases is that they are generally nanocrystalline or amorphous (as indicated by the hump in Figure 5) in the as-sprayed form, and fully crystallized in the heat-treated conditions. The role of carbide matrix in terms of ductility and its bond strength with the carbides therefore requires further research. The role of residual stress profile on the fracture response of the coating [51] and its dependence on the structure of the nanosized particles observed in suspension spraying also requires further investigations. However, this investigation shows that the size and nature of carbides in the wear debris dominated the wear mechanism in three-body abrasion, and was the main contributing factor for the differences in the wear rate observed for the steel ball counterface (Figure 10). The sliding

wear rate against steel ball couple in this investigation can also be compared against a recently reported investigation of another S-HVOF coating using milled conventional WC-Co powder [41]. This comparison indicated relatively better wear rate in the current investigation due to nano-carbides in the start powder.

For the case of HVOF-JK coatings, erosion of cobalt-based matrix (Figure 7g) was observed, which left the larger carbides unprotected leading to carbide pull-out. Carbide fracture was also detected for the HVOF-JK coatings (Figure 7d). In comparison, preferential wear of matrix and carbide fracture was not perceived in the S-HVOF coatings. It is however possible that at higher loads, the wear mechanism of S-HVOF coatings may be dominated by fracture, as indicated by Shipway et al. [1], however it was not observed under the tribological test conditions in this investigation. This may be attributed to the improved quality of S-HVOF coatings using aqueous suspensions as opposed to the conventional HVOF coatings in the previous investigation [1]. The role of wear debris in three-body abrasion was also seen on the ball-scar surface (Figure 12 a,b), where the abrasion marks in different directions can be observed. Embedded debris and dents caused by the WC particles were also detected on the steel ball surface. The debris in the S-HVOF coatings are expected to originate from nanosized particles, where the relative hardness of these particles will range from lower values for W to WC and higher values for M_6C and $M_{12}C$ (eta-phases). Hence in comparing S-HVOF and HVOF-JK coatings; both of these factors i.e. i) the smaller carbide size (nanosized particles) in the wear debris which are predominantly W and WC in comparison to predominantly larger WC carbides for HVOF-JK, and ii) support of metal matrix for the nanosized particles which is similar to the effect of lower binder mean free path of the metal matrix as indicated by Houdková et al. [12] and Chivavibul et al. [28], resulted in a lower wear rate for both the ball and coating materials for the S-HVOF coatings (Figure 10).

Comparison of the wear rate for the third generation HVOF-JP coatings with the first generation HVOF systems (HVOF-JK) and second generation (TopGun) modified for S-HVOF process, indicated that the ball wear rate was minimal for the HVOF-JP coatings (Figure 10). This is attributed to the higher hardness (Table 4) and fracture toughness ($7.4 \pm 0.5 \text{ MPa m}^{1/2}$) of the HVOF-

JP coatings [43,50], which resulted in relatively less carbide debris and ball wear. The tribofilm and a lower concentration of WC particles in the wear debris therefore protected the ball surface. The quandary however was the relatively higher wear rate of the HVOF-JP coatings against the steel ball surface. This requires further investigation, however it is postulated that towards the end of the wear test, the HVOF-JP coating delaminated due to fatigue (fracture driven mechanism as opposed to the erosion of matrix and carbide pull-out), as shown in Figure 7f. If this delamination occurred towards the end of the wear test, the wear debris will not have sufficient time to accelerate ball wear.

The friction coefficient record comparison of the S-HVOF and HVOF-JK coatings revealed in Figure 11a, indicate a similar steady state friction coefficient values. The frictional behavior of the HVOF-JK coatings was relatively more uniform throughout the test duration, indicating that the dominant wear mechanism for the S-HVOF coatings varied throughout the test. Initial lower values may be associated with the formation of transfer film, whereas higher values at the later stages before steady state friction can be expected to be dominated by two and three-body abrasion. The steady state friction values of HVOF-JP coatings were higher than that of HVOF-JK coating, with average steady state friction coefficient of 0.58. This relatively high friction coefficient on a hard and relatively tough HVOF-JP coating may indicate the possibility of the shift in wear mechanism to delamination. This however requires further investigation.

5.2.2 *Comparison between S-HVOF, HVOF-JK and HVOF-JP coatings against WC-Co balls*

Sliding wear resistance of the HVOF WC-Co coatings against the WC-Co counterface has been widely reported. A recent investigation by Wood [4] summarizes some of these studies where sintered carbides, HVOF coatings and spark plasma sintered (SPS) WC-Co coatings have been tested against the WC ball or pin. Wood [4] reported that for the case of WC counterbody, the wear rate is dependent upon the aforementioned factors of WC particle size, WC content and bonding of the WC particle with the cobalt matrix. A more uniform distribution of carbides in the matrix is also a contributing factor in reducing the wear rate. Wood [4] reported that the wear mechanism in the case of WC counterbody was dominated by the carbide pull-out and /or tribofilm. Despite this

similarity in the dominant factors influencing wear rate and the wear mechanism, there are some subtle differences when comparing the wear performance between the steel and the WC-Co ball counterface materials.

The WC-Co ball was almost four times harder than the steel ball ($HV_{0.3} \approx 1650$) and its fracture toughness ($7.8 \text{ MPa m}^{1/2}$) was almost 1/12 of the steel ball. Similarly the elastic modulus of WC-Co ball (580 GPa) was almost 2.75 times that of the steel ball. This indicates that the wear of WC-Co ball and coating will be more dominated by the erosion of binder phase and the higher stress level during the test. The Hertzian contact stress (P_o) at the start of the sliding wear test was 1.18 GPa and 1.86 GPa for the steel and WC-Co balls, respectively. Based on the wear scar diameter, the average contact pressure at the end of the test was approximated as $7.5 \pm 1 \text{ MPa}$ and $30 \pm 15 \text{ MPa}$, respectively. The actual contact pressure at the end of the sliding wear test will be relatively higher than these values ($7.5 \pm 1 \text{ MPa}$ and $30 \pm 15 \text{ MPa}$, respectively) for both coatings, due to the role of the wear debris, as they cause differences in the real and apparent area of contact. However the relative stress will be higher for the case of WC-Co ball, not only because the apparent area of contact is lower due to lower WC-Co ball wear (or wear track width), but also because the debris in the contact will be predominantly WC (or nanosized particles) as opposed to a combination of WC (or nanosized particles) and Fe for the steel ball. Given the higher stress and hardness of carbides in the wear debris for the couples involving WC-Co ball, the ball and coating wear is expected to be higher. The higher hardness and toughness of the WC-Co ball in comparison to the coating compensates this harder third body in the contact region, resulting in a relatively lower WC-Co ball volume loss in comparison to the steel ball. Once again, the nanosized particles in the wear debris, and their composition of predominantly W and WC for S-HVOF coatings results in the lowest ball volume loss when compared to the HVOF-JK and HVOF-JP coatings (Figure 10). This also results in the lowest total wear rate for the S-HVOF coatings followed by HVOF-JK and HVOF-JP coatings. The wear rate for the S-HVOF coatings against the WC-Co ball was the highest with high standard deviation, indicating that the presence of the larger and harder ball debris in the contact region accelerated the wear of nanosized particles in the S-HVOF coating. This can be observed in Figures 8a,b,c indicating severe abrasion and fracture of the wear track. The tribofilm resulting

from oxidized particles indicated 20 wt.% oxygen (Figure 8c). The WC-Co ball wear surface (Figure 12c,d) indicated a relatively smoother surface with some extrusion of cobalt matrix. The wear debris (Figure 13b) resulting from the WC-Co ball and coating surfaces had a plate like morphology with relatively bigger particle size in comparison to the steel ball wear debris (Figure 13a) which resulted from coating fracture.

In comparison to the S-HVOF coatings, the wear tracks of the HVOF-JK and HVOF-JP coatings against the WC-Co ball indicated less severe wear (Figures d,e,f,g) and tribofilm. The coating wear rate was also relatively less than that of S-HVOF coatings. However the lower ball volume loss of S-HVOF coatings resulted in a lower total wear rate for the S-HVOF coating when tested against the WC-Co ball. Relatively lower tribofilm formation on the surface of the HVOF-JP coatings also indicated relatively higher friction values as shown in Figure 11b. The frictional behavior of HVOF-JK coatings against the WC-Co ball was similar to that of HVOF-JP coatings.

5.2.3 *Comparison between S-HVOF, HVOF-JK and HVOF-JP coatings against Si₃N₄ ceramic balls*

Although the fracture toughness ($6 \text{ MPa m}^{1/2}$) and hardness ($\text{HV}_{0.3} \approx 1550$) of the Si₃N₄ ceramic balls was comparable to that of WC-Co balls, the wear rate of the test-couples involving these ceramic balls was in between the steel and WC-Co balls (Figure 10). This is attributed to the tribo-chemistry of Si₃N₄ which results in relative softening of the surface, and the resulting tribofilm is expected to have good lubricating properties [52]. As the sliding wear experiments were performed in air, the air moisture content and the flash temperatures at asperity levels resulted in the formation of tribofilm as observed on the ball surface (Figure 12f). The EDX analysis of the wear track on the ball surface did not indicate presence of WC or Co, indicating that there was no transfer layer from the coating surface. Hence the mechanism of ball wear for the Si₃N₄ ceramic was different in comparison to the WC-Co and the steel ball due to the action of moisture in air. Further details of these tribo-chemical reactions associated with the Si₃N₄ ceramic can be seen in a recent detailed review [52]. Although the ball wear rate for the Si₃N₄ ceramic was similar for the S-HVOF and HVOF-JK coatings, the coating volume loss was the highest for the S-HVOF coatings. This is in

contrast to the lowest friction coefficient recorded for S-HVOF coatings against the Si_3N_4 ceramic balls (Figure 11c). The higher coating wear rate for S-HVOF coatings for the tests against the Si_3N_4 ceramic ball is attributed to the microscale preferential wear of the coating matrix, exposing the nanosized particles as shown in Figure 9. The tribo-chemical reaction of the Si_3N_4 ceramic leaves finer debris which preferentially can wear the matrix in cemented carbides through microscale abrasion, as reported previously by Shipway and Hogg [6].

5.2.4 *Structure-property relationships*

Wayne et al. [53] has indicated that the abrasive wear rate for a range of sintered WC-Co cermets is approximately proportional to a function of $D_{\text{WC}} / (K_{\text{IC}}^{3/8} H^{1/2})$, where D_{WC} is the average WC grain size, H hardness of WC-Co and K_{IC} its fracture toughness. This correlation was based on the wear mechanism which initiated from the cobalt extrusion followed by the carbide removal. In the current investigation although the average carbide size varied between the S-HVOF and HVOF coatings, the proportionality of wear rate to $D_{\text{WC}} / (K_{\text{IC}}^{3/8} H^{1/2})$ was not observed. This is attributed to the non-sintered nature of carbides in thermally sprayed WC-Co coatings, and to the changes in the wear mechanism when considering the steel, Si_3N_4 ceramic and WC-Co ball surfaces. Such relationships normally do not follow beyond the specific tribological test conditions which normally involve the same type of test couples. In the current investigation, the changes in ball material and hence the changes in wear mechanism(s), added additional complexity to the task of relating mechanical properties to the tribological wear performance. Wood [4] has also recently indicated this complexity and indicated that in the case of thermal spray coatings, the dependencies of wear rate on the binder metal, porosity, hardness and Young's modulus were not found.

In the current investigation, as the ball material varies significantly in terms of its relative hardness (H_{ball}), Young's modulus (E_{ball}), fracture toughness ($K_{\text{IC ball}}$) when compared to the respective coating hardness (H_{coating}), Young's modulus (E_{coating}) and fracture toughness ($K_{\text{IC coating}}$), a linear relationship satisfying all tribological conditions considered in this investigation was not achievable. Instead, an effort was made to incorporate the influence of critical factors such as:

- i) normally in sliding wear applications the hardness of the harder counterface is used. However in the current investigation of HVOF coatings, as the relative ball hardness is lower for the steel and higher for the WC-Co and Si₃N₄, an attempt is made to incorporate the influence of the ball to the coating hardness ratio ($H_{ball}/H_{coating}$),
- ii) as the ball diameter was relatively smaller for the WC-Co ball in comparison to the steel and Si₃N₄ ceramic balls, and as the values of the elastic properties varied between the various test couples, a variable based upon the Hertzian contact stress (P_o) was introduced to cater for the differences in the ball geometry and elastic properties of test couples,
- iii) fracture of surfaces inevitably leads to the formation of wear debris so the K_{IC} of the coatings was considered as another variable.

The fracture toughness of the ball material was not directly included in this analysis as for the steel and WC-Co balls, fracture dominated wear mechanism was not observed. The fracture dominance of the hydrated Si₃N₄ ceramic tribofilm was also not clear to be included as a variable in this analysis. The above variables although cater for most of the wear mechanisms, the lack of data on the yield strength of hydrated Si₃N₄ film meant that plasticity could only be introduced indirectly in the form of hardness ratio. It may be possible to investigate the mechanical properties of hydrated Si₃N₄ film using nanoindentation and nanoscratch tests [54-55]. Similarly, the carbide size and carbon loss in the coating microstructure was indirectly used in the form of coating fracture toughness values.

Figure 14, provides some basic correlations between the tribological and structural (microstructure and mechanical) properties. Figure 14a shows the simple correlation between the wear rate and contact stress. This correlation provides very similar linear fits for the S-HVOF and HVOF-JK coatings. Figure 14b shows the wear rate correlation with the $\sqrt{\frac{H_{ball}}{H_{coating}}} \times E_{ball} / \sqrt{K_{IC\ coating}}$ variable. In this correlation, the linear fit is within the standard deviation of the experimental wear rates for the HVOF-JP and HVOF-JK coatings, whereas for the case of S-HVOF coatings the linear function fits with less accuracy. Figure 14c shows a

modified correlation of the total wear rate with $\left(\frac{H_{ball}}{H_{coating}}\right)^{3/4} \times \left(\frac{P_0}{H_{ball}}\right)^{2/3} / \sqrt{K_{IC\ coating}}$. This correlation provides a similar fit for both the S-HVOF and HVOF-JK coatings. Although these correlations fall within the standard deviation of the experimental wear rates of the sliding wear tests, a better fit could not be achieved if carbide size was introduced as a variable, as proposed by Wayne et al. [53].

6. CONCLUSIONS

- 1) Dense nanostructured coatings with hardness up to 942 ± 15 HV_{0.3} have been deposited by S-HVOF spraying using an aqueous suspension of a milled nanostructured WC-Co feedstock which had some eta-phases. The microstructure of the as-sprayed S-HVOF coatings indicated nanosized particles (WC, W, M₆C, M₁₂C) some of which were inherited from the milled powder, whereas others formed as a result of carbon loss, demonstrating that the S-HVOF process retained the nanocomposite features during coating deposition.
- 2) A comparison of the S-HVOF and conventional HVOF coatings points toward phase transformations occurring in the S-HVOF coating process which led to the nanostructured and amorphous phases. This phase transformation in the conventional HVOF coatings was relatively lower.
- 3) After heat treatment at 920 °C WC, metallic tungsten and two η-phases M₆C (Co₂W₄C) and M₁₂C (Co₆W₆C) were observed in the X-ray diffraction pattern of the S-HVOF coating.
- 4) Sliding wear evaluations indicated that the performance was test-couple dependent, with HVOF-JP coatings performing the best against the steel and ceramic couples, whereas the improved performance for the S-HVOF coatings was observed when tested against the WC-Co ball.
- 5) Total wear rate was dominated by the ball wear. A higher ball wear rate was generally observed with a relatively lower coating wear rate.
- 6) The dominant wear mechanism was matrix erosion followed by the carbide (or nanosized particle) pull out and coating fracture. Tribofilm formation was also observed in all test couples. Fracture of carbides was also detected for the HVOF-JK coatings.

- 7) There was preferential abrasion of metal matrix in the conventional HVOF-JK coatings.
- 8) Structure property correlations indicate that the correlations based on the contact stress, hardness ratio and fracture toughness can provide a linear fit within the limits of the standard deviation of the experimental wear data.

7. REFERENCES

- [1] P.H. Shipway, D.G. McCartney, T. Sudaprasert, Sliding wear behaviour of conventional and nanostructured HVOF sprayed WC–Co coatings, *Wear* 259 (2005) 820–827.
- [2] Q. Yang, T. Senda, A. Ohmori, Effect of carbide grain size on microstructure and sliding wear behavior of HVOF-sprayed WC–12% Co coatings, *Wear* 254 (2003) 23–34.
- [3] V. Rajinikanth, K. Venkateswarlu, An investigation of sliding wear behavior of WC–Co coating, *Tribology International* 44 (2011) 1711–1719.
- [4] R. J.K. Wood, Tribology of thermal sprayed WC–Co coatings, *Int. Journal of Refractory Metals & Hard Materials* 28 (2010) 82–94.
- [5] H. Engqvist, H. Högberg, G.A. Botton, S. Ederyd, N. Axén, Tribofilm formation on cemented carbides in dry sliding conformal contact, *Wear* 239 (2000). 219–228.
- [6] P.H. Shipway, J.J. Hogg, Dependence of microscale abrasion mechanisms of WC-Co hardmetals on abrasive type, *Wear* 259 (2005) 44–51.
- [7] Z.Z. Fang, X. Wang, T. Ryu, K.S. Hwang, and H.Y. Sohn, Synthesis, Sintering, and Mechanical Properties of Nanocrystalline Cemented- A Review, *International Journal of Refractory Metals & Hard Materials*, 2009, 27, p 288-299
- [8] L.-M. Berger, in: *Comprehensive Hard Materials*, Volume 1, Hardmetals, V. Sarin, D. Mari, L. Llanes, C. Nebel (eds), Elsevier, Amsterdam, 2014, p 479-514
- [9] V. Stoica, R. Ahmed, T. Itsukaichi, and S. Tobe, Sliding Wear Evaluation of HIPed Thermal Spray Cermet Coatings, *Wear*, 2004, 257(11), p 1103-1124
- [10] S. Stewart, R. Ahmed, and T. Itsukaichi, Rolling Contact Fatigue of Post-treated WC-NiCrBSi Thermal Spray Coatings, *Surface and Coatings Technology*, 2005, 190(2-3), p 171-189
- [11] R. Ahmed, and M. Hadfield, Mechanisms of Fatigue Failure in Thermal Spray Coatings, *Journal of Thermal Spray Technology*, 2002, 11(3), p 333-349

- [12] Š. Houdková, F. Zahálka, M. Kašparová, and L.-M. Berger, Comparative Study of Thermally Sprayed Coatings Under Different Types of Wear Conditions for Hard Chromium Replacement, *Tribology Letters*, 2011, 43, p 139-154
- [13] Vuoristo, P., Niemi, K., Mäntylä, T., Berger, L.-M., Nebelung, M., Comparison of Different Hardmetal-like Coatings Sprayed by Plasma and Detonation Gun Processes, *Adv. Thermal Spray Sci. Technol., Proc. 8th Nat. Therm. Spray Conf.*, 11-15 September 1995, Houston, Ed. by C.C: Berndt and S. Sampath (Eds.), ASM International, Materials Park, 1995, 309-315.
- [14] V. Bonache, M.D. Salvador, J.C. García, E. Sánchez, and E. Bannier, Influence of Plasma Intensity on Wear and Erosion Resistance of Conventional and Nanometric WC-Co Coatings Deposited by APS, *Journal of Thermal Spray Technology*, 2011, 20(3), p 549-559
- [15] E. Sánchez, E. Bannier, M.D. Salvador, V. Bonache, J.C. García, J. Morgiel, and J. Grzonka, Microstructure and Wear Behavior of Conventional and Nanostructured Plasma-Sprayed WC-Co Coatings, *Journal of Thermal Spray Technology*, 2010, 19(5), p 964-974
- [16] G. Bolelli, V. Cannillo, L. Lusvarghi, R. Rosa, A.V. Wanhuk, B. Choib, R. Dey, C. Weyant, S. Sampath, Functionally Graded WC-Co/NiAl HVOF Coatings for Damage Tolerance, *Wear and Corrosion Protection, Surface and Coatings Technology*, 2012, 206(8-9), p 2585-2601
- [17] H. Chen, G. Gou, M. Tu, and Y. Liu, Research on the Friction and Wear Behavior at Elevated Temperature of Plasma-Sprayed Nanostructured WC-Co Coatings, *Journal of Materials Engineering and Performance*, 2010, 19(1), p 1-6
- [18] H.L. de Villiers Lovelock, Powder/Processing/Structure Relationship in WC-Co Thermal Spray Coatings: A Review of the Published Literature, *Journal of Thermal Spray Technology*, 1998, 7(3), pp 357-373
- [19] S. Stewart, and R. Ahmed, Contact Fatigue Failure Modes in Hot Isostatically Pressed WC-12%Co Coatings, *Surface and Coatings Technology*, 2003, 172, p 204-216
- [20] V. Stoica, and R. Ahmed, Influence of Vacuum Heat Treatment on Sliding Wear of Thermal Spray Cermet Coatings, *Surface and Coating Technology*, 2005, 199(1), p 7-21

- [21] V. Stoica, R. Ahmed, T. Itsukaichi, and S. Tobe, Sliding Wear Evaluation of Hot Isostatically Pressed (HIPed) Thermal Spray Cermet Coatings, *Wear*, 2004, 257(11), p 1103-1124
- [22] V. Stoica, R. Ahmed, and S. Tobe, Wear of Hot Isostatically Pressed (HIPed) Thermal Spray Cermet Coatings, *Journal of Thermal Spray Technology*, 2004, 13(1), p 93-107
- [23] Berger, L.-M., Saaro, S., & Woydt, M. (2007). Reib-/Gleitverschleiß von thermisch gespritzten Hartmetallschichten, In R. Suchentrunk (Ed.), *Jahrbuch Oberflächentechnik 2007, Vol. 63*, (pp. 242–267). Bad Saulgau: Eugen G. Leuze Verlag.
- [24] Berger, L.-M., Woydt, M. and Saaro, S. (2009) Comparison of self-mated hardmetal coatings under dry sliding conditions up to 600 °C, *Wear* 266 (3-4), 406-416.
- [25] Berger, L.-M., Stahr, C.C., Saaro, S., Thiele, S., Woydt, M., and Kelling, N. (2009) Dry sliding up to 7.5 m/s and 800°C of thermally sprayed coatings of the TiO₂-Cr₂O₃ System and (Ti,Mo)(C,N)-Ni(Co), *Wear* 267 (5-8), 954-964.
- [26] Bolelli G, Berger L-M, Bonetti M, Lusvardi L. Comparative study of the dry sliding wear behaviour of HVOF-sprayed WC-(W,Cr)₂C-Ni and WC-CoCr hardmetal coatings. *Wear* 309 (1-2), 2014, 96-111.
- [27] J. He, J. M. Schoenung, A review on nanostructured WC–Co coatings, *Surface and Coatings Technology*, 157(1), 2002, p72–79.
- [28] P. Chivavibul, M. Watanabe, S. Kuroda, and K. Shinoda, Effects of Carbide Size and Co Content on the Microstructure and Mechanical Properties of HVOF-Sprayed WC–Co Coatings, *Surface & Coatings Technology*, 2007, 202 (3), p 509-521
- [29] P. Fauchais, G. Montavon, R.S. Lima, and B.R. Marple, Engineering a New Class of Thermal Spray Nano-based Microstructures from Agglomerated Nanostructured Particles, Suspension and Solutions: An Invited Review, *Journal of Physics D: Applied Physics*, 2011, 44, art no. 093001 (53 pp).
- [30] V. Chawla, B.S. Sidhu, D. Puri, and S. Prakash, State of Art: Plasma Sprayed Nanostructured Coatings: A Review, *Materials Forum*, 2008, 32, p 137-143
- [31] J. He, and J.M. Schoenung, Review-Nanostructured Coatings, *Materials Science and Engineering A*, 2002, 336, p 274-319

- [32] J. Oberste Berghaus, B. Marple, and C. Moreau, Suspension Plasma Spraying of Nanostructured WC-12Co Coatings, *Journal of Thermal Spray Technology*, 2006, 15, p 676-681
- [33] L.-M. Berger, F.-L. Toma, and A. Potthoff, Thermal Spraying with Suspensions-An Economic Spray Process, *Thermal Spray Bulletin*, 2013, 6(2) p 98-101
- [34] F.-L. Toma, L.-M. Berger, S. Langner, and T. Naumann, Suspension Spraying-The Potential of a New Spray Technology, *Thermal Spray Bulletin*, 2010, 3(1), p 24-29.
- [35] F.-L. Toma, L.-M. Berger, C.C. Stahr, T. Naumann, and S. Langner, Microstructures and Functional Properties of Suspension-Sprayed Al₂O₃ and TiO₂ Coatings: An Overview, *Journal of Thermal Spray Technology*, 2010, 19(1-2) , p 262-274
- [36] P. Fauchais, G. Montavon, Latest Developments in Suspension and Liquid Precursor Thermal Spraying, 2010, 19(1-2), p 226–239
- [37] P. Fauchais, A. Vardelle, Innovative and Emerging Processes in Plasma Spraying: From Micro-to Nanostructured Coatings, *Journal of Physics D: Applied Physics*, 2011, 44, art no. 194011 (14pp)
- [38] K. Korpiola, High Temperature Oxidation of Metal, Alloy and Cermet Powders in HVOF Spraying Process, Dissertation, Helsinki University of Technology, 2006.
- [39] Bolelli, G., Cannillo, V., Gadov, R., Killinger, A., Lusvarghi, L., Rauch, J. (2009). Properties of High Velocity Suspension Flame Sprayed (HVSFS) TiO₂ Coatings, *Surf. Coat. Technol.*, 203 (12), 1722-1732.
- [40] Bolelli, G., Rauch, J., Cannillo, V., Killinger, A., Lusvarghi, L., V., Gadov, R. (2009). Microstructural and Tribological Investigation of High-Velocity Suspension Flame Sprayed (HVSFS) Al₂O₃ Coatings, *J. Therm. Spray Technol.*, 18 (1), 35-49.
- [41] R. Ahmed, N. H. Faisal, Nayef M. Al-Anazi, S. Al-Mutairi, F.-L. Toma, L.-M. Berger, A. Potthoff, E. K. Polychroniadis, M. Sall, D. Chaliampalias, M. F. A. Goosen, “Tribomechanical Evaluation of Suspension Thermal Sprayed WC-Co Nanocomposite Coatings”, *Journal of Thermal Spray Technology*, In print 2014.
- [42] F.-L. Toma, L.-M. Berger, S. Scheitz, S. Langner, C. Rödel, A. Potthoff, V. Sauchuk, and M. Kusnezoff, Comparison of the Microstructural Characteristics and Electrical Properties

of Thermally Sprayed Al_2O_3 Coatings from Aqueous Suspensions and Feedstock Powders, *Journal of Thermal Spray Technology*, 2012, 21(3-4), p 480-488

- [43] N. H. Faisal, J. A. Steel, R. Ahmed and R. L. Reuben, The Use of Acoustic Emission (AE) to Characterise Vickers Indentation Behaviour of HVOF Thermally Sprayed WC-12%Co Coatings, *Journal of Thermal Spray Technology*, 2009, 18(4), p 525-535
- [44] Gärtner, F., Kreye, H. and Richter, H.J. (2006) HVOF spraying with powder and wire, Proc. 7th Kolloquium Hochgeschwindigkeitsflammspritzen, 9.-10.11.2006, Erding, Germany, Unterschleißheim, Gemeinschaft Thermisches Spritzen, 39-56.
- [45] S. Osawa, T. Itsukaichi and R. Ahmed, "Influence of Powder Size and Strength on HVOF Spraying - Mapping the Onset of Spitting", *Advancing the Science and Applying the Technology*, International Thermal Spray Conference, Florida, USA, pp. 819-824, 2003.
- [46] S. Thiele, K. Sempf, K. Jaenicke-Roessler, L.-M. Berger, and J. Spatzier, Thermophysical and Microstructural Studies on Thermally Sprayed Tungsten Carbide-Cobalt Coatings, *Journal of Thermal Spray Technology*, 2011, 20(1-2), p 358-365
- [47] C. Verdon, A. Karimi, J.-L. Martin, A Study of High Velocity Oxy-Fuel Thermally Sprayed Tungsten Carbide Based Coatings. Part 1: Microstructures, *Mater. Sci. Engineer.* 1998, A246 (1-2), 11-24.
- [48] D.A. Stewart, P.H. Shipway, D.G. McCartney, Microstructural Evolution in Thermally Sprayed WC-Co Coatings: Comparison between Nanocomposite and Conventional Starting Powders, *Acta Mater.*, 2000, 48 (7), 1593-1604.
- [49] A.S. Kurlov, and A.I. Gusev, *Tungsten Carbides: Structure, Properties and Application in Hardmetals*. Cham etc.: Springer; 2013.
- [50] N. H. Faisal, R. Ahmed, S. B. Spence, M. Hossain, J. A. Steel, "An improved model to assess the quality of thermally sprayed coatings under Vickers indentation", *Engineering Fracture Mechanics*, In press, 2014.
- [51] R. Ahmed, H. Yu, L. Edwards and J. Santisteban, "Neutron Diffraction Residual Strain Measurements in Post-treated Thermal Spray Cermet Coatings", *Material Science and Engineering-A*, Vol. 498, pp. 191-202, 2008.

- [52] R. C. Dante, C.K. Kajdas, A review and a fundamental theory of silicon nitride tribochemistry, *Wear* 288 (2012) 27– 38.
- [53] S. F. Wayne, J. G. Baldoni, S. T. Buljan, Abrasion and erosion of WC-Co with controlled microstructures, *Tribology transactions* 33(4), 1990, 611-617.
- [54] R. Ahmed, A. Ashraf, M. Elameen, N. H. Faisal, A. M. El-Sherik, Y. O. Elakwah, M. F. A. Goosen, “Single Asperity Nanoscratch Behavior of HIPed and Cast Stellite 6 Alloys”, *Wear*, <http://dx.doi.org/10.1016/j.wear.2014.02.006>, Volume 312, Issues 1–2, 15 April 2014, Pages 70–82.
- [55] N. H. Faisal, R. Ahmed and R. L. Reuben, “Indentation testing and its acoustic emission response: applications and emerging trends”, *International Materials Reviews*, Vol. 56(2), pp. 98-142, 2011.

TABLES and FIGURES

Table 1, Parameters calculated from particle size distributions and BET for as-received and milled WC-Co powders

Material	$x_{10;3}$ [μm]	$x_{50;3}$ [μm]	$x_{90;3}$ [μm]	BET [m^2/g]
WC-Co (As-received powder)	1.95	9.1	21.5	0.90
WC-Co (Milled powder)	2.50	4.0	6.4	20.0

Table 2: Spray parameters used for WC-Co S-HVOF spraying

Spray condition #	C_2H_4 (l/min)	O_2 (l/min)	$\text{C}_2\text{H}_4/\text{O}_2$ ratio	Spray distance (mm)
S-HVOF # 1	75	175	0.77	90
S-HVOF # 2	75	190	0.84	90
S-HVOF # 3	65	165	0.84	80
S-HVOF # 4	75	170	0.75	90

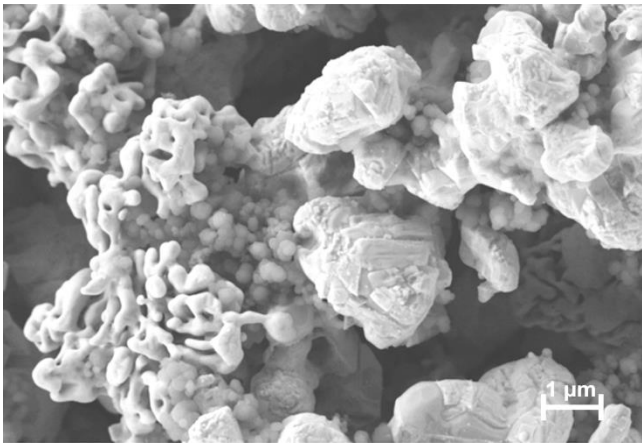
Table 3: Spray parameters used for WC-Co HVOF-JP spraying

Process/System	Oxygen flow [l/min]	Kerosene flow [l/min]	Spraying rate [g/min]	Spraying distance [mm]
HVOF/ JP5000	893	0.32	70	380

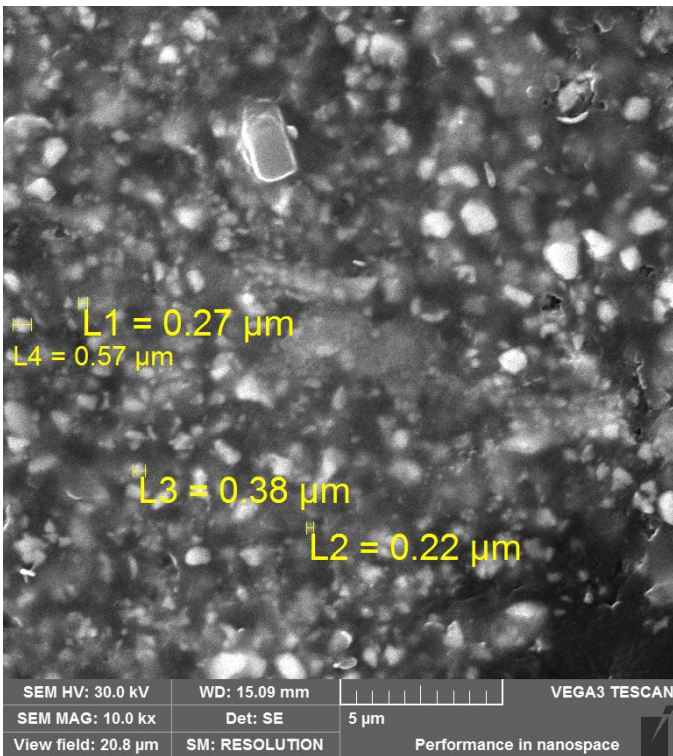
Table 4, Coating thickness and Vickers hardness values for S-HVOF, HVOF-JK, and HVOF-JP coatings

# Sample	Av. coating thickness (μm)	Av. coating thickness per pass ($\mu\text{m}/\text{pass}$)	Hardness HV0,3
S-HVOF (Spray condition # 1)	180	4.5	891 \pm 24
S-HVOF (Spray condition # 2)	200	5.0	918 \pm 34
S-HVOF (Spray condition # 3)	95	2.5	773 \pm 19*
S-HVOF (Spray condition # 4)	210	3.1	942 \pm 15
HVOF-JK	330	-	924 \pm 127
HVOF-JP	400	-	1118 \pm 131

* indicative value due to relatively lower coating thickness



a



b

Figure 1, SEM Image of the a) as-received b) cross-section of the milled WC-12Co powders.

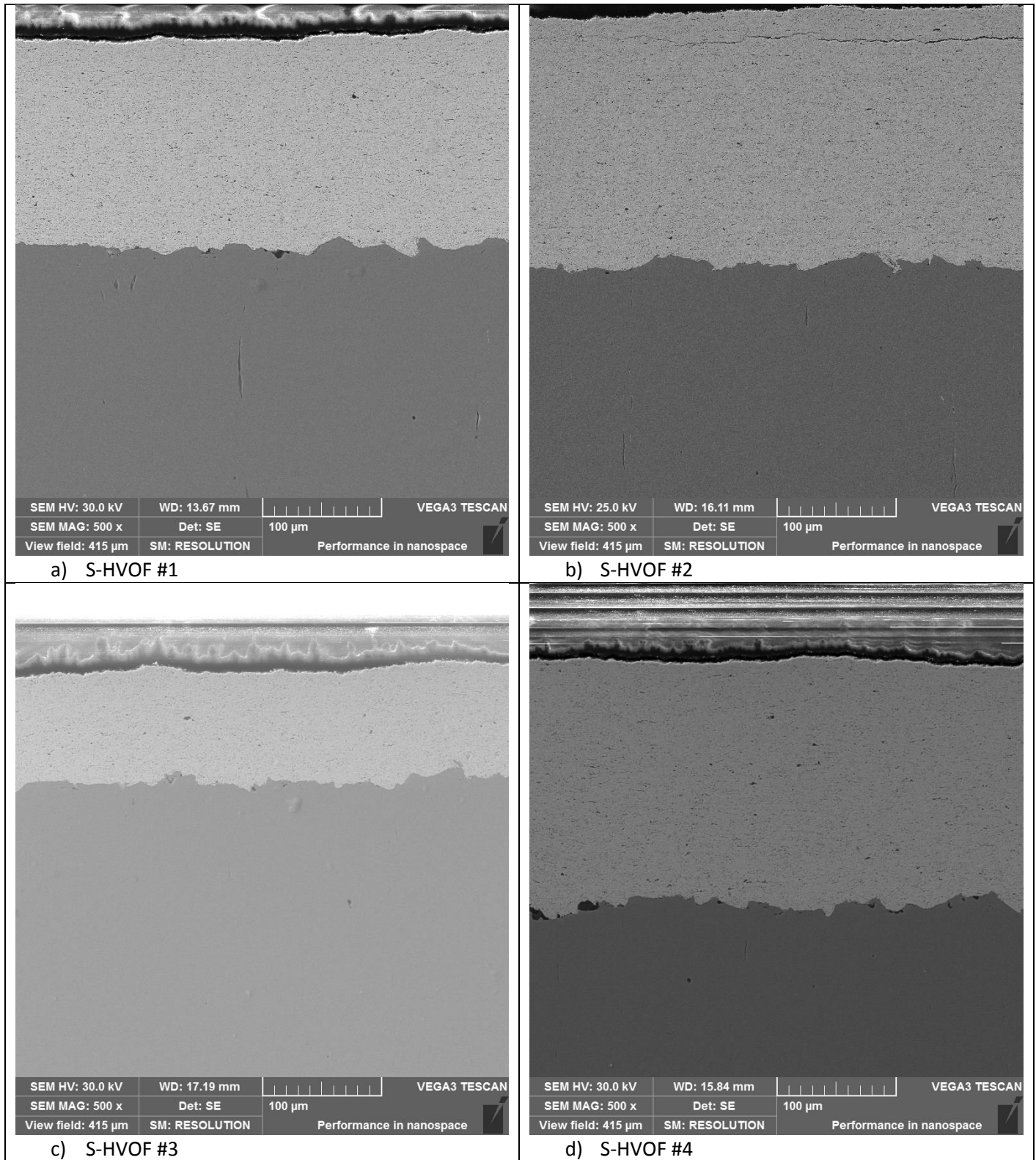
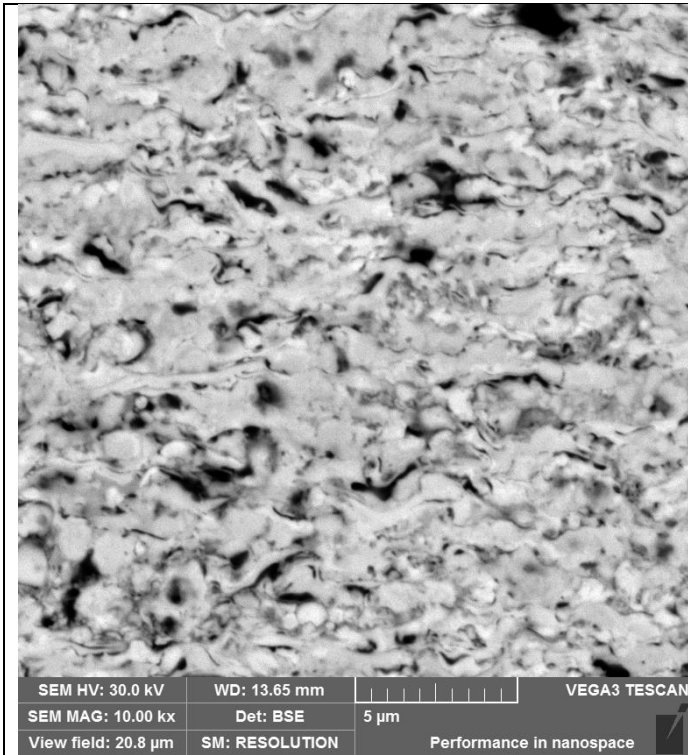
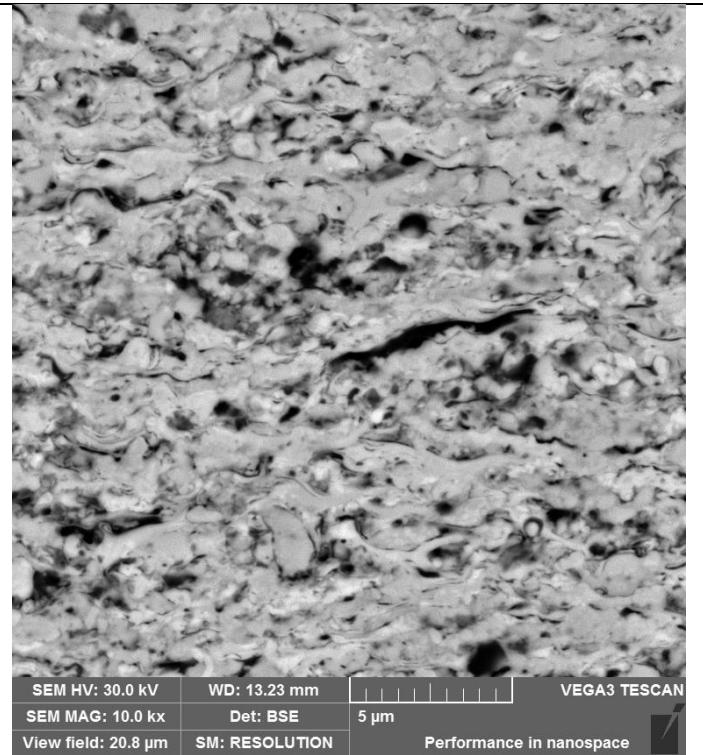


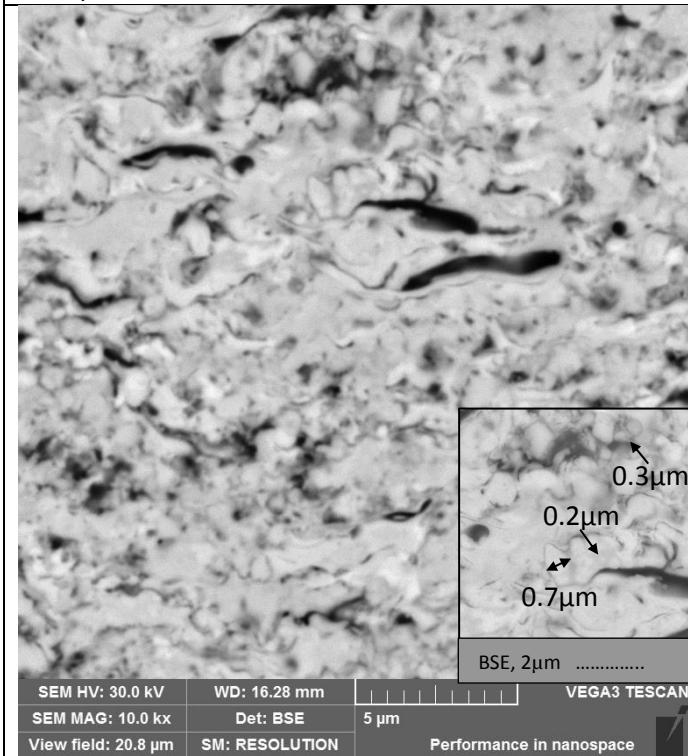
Figure 2, SEM observation of the coating substrate system deposited by the S-HVOF spraying



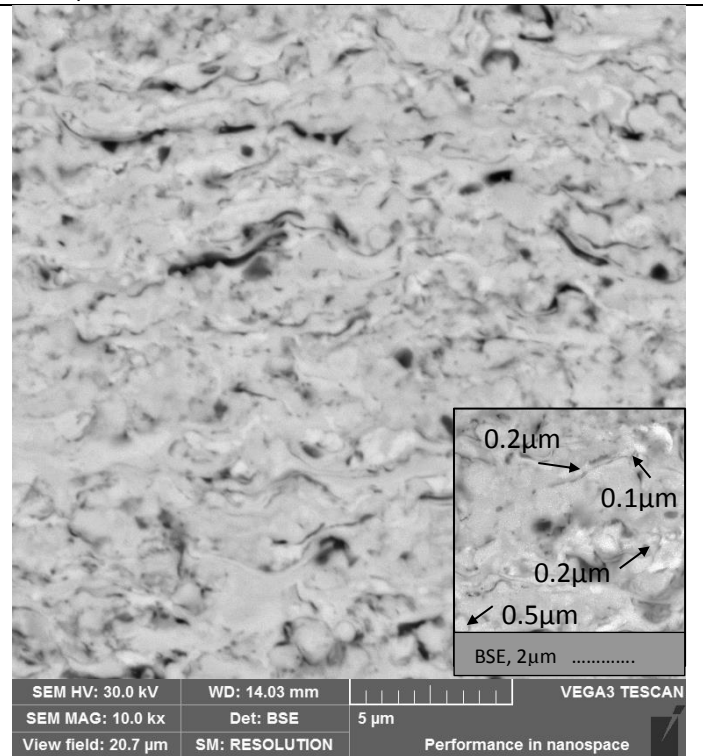
a) S-HVOF #1



b) S-HVOF #2

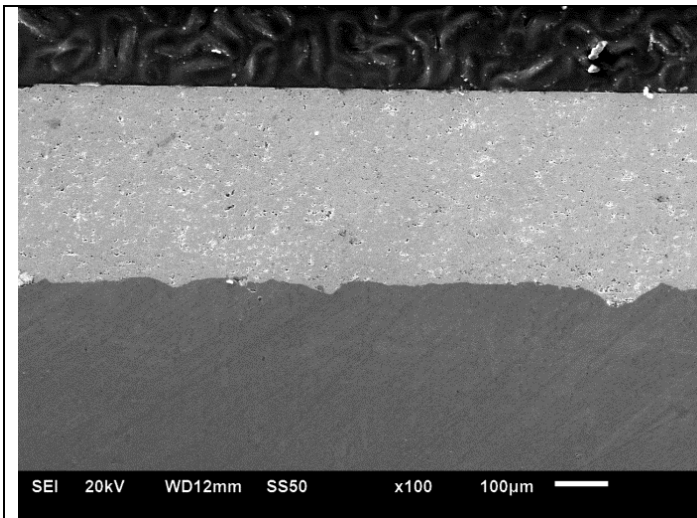


c) S-HVOF #3, inserts indicate higher magnification (30 kx) images

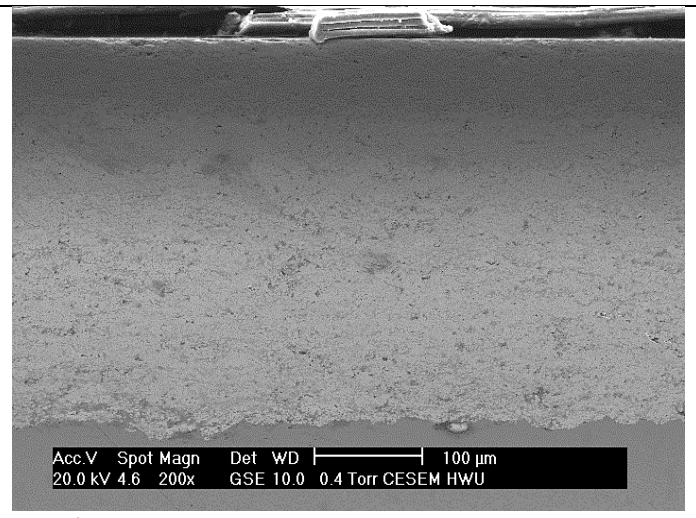


d) S-HVOF #4, inserts indicate higher magnification (30 kx) images

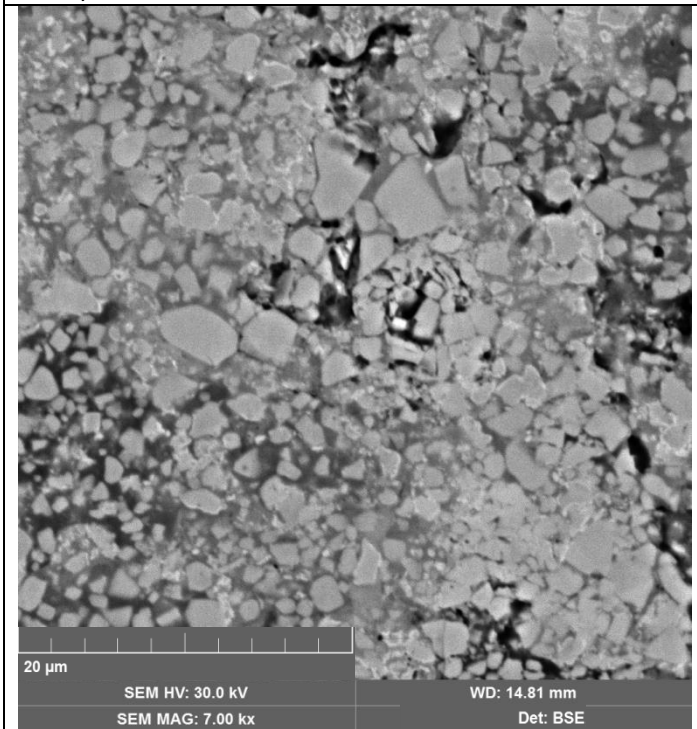
Figure3, Higher magnification SEM images of the S-HVOF coatings



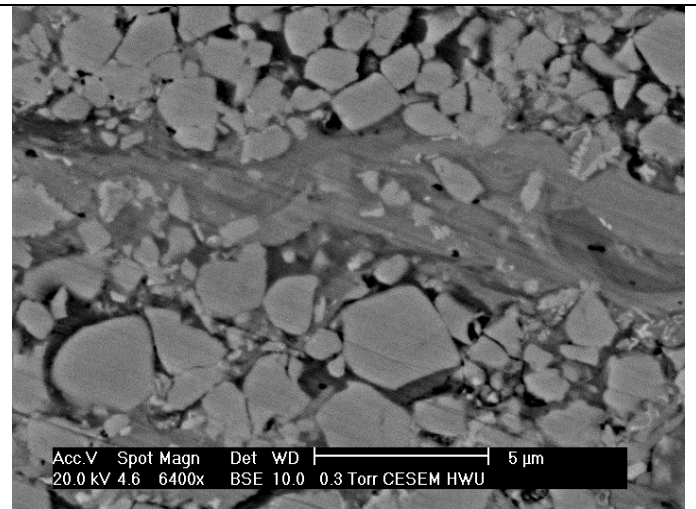
a) HVOF-JK



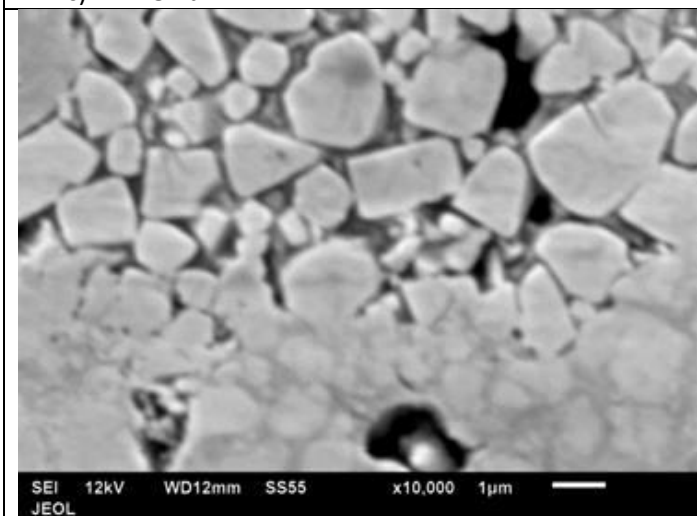
b) HVOF-JP



c) HVOF-JK



d) HVOF-JP



e) HVOF-JK

Figure 4, Higher magnification SEM images of the HVOF-JK and HVOF-JP coatings

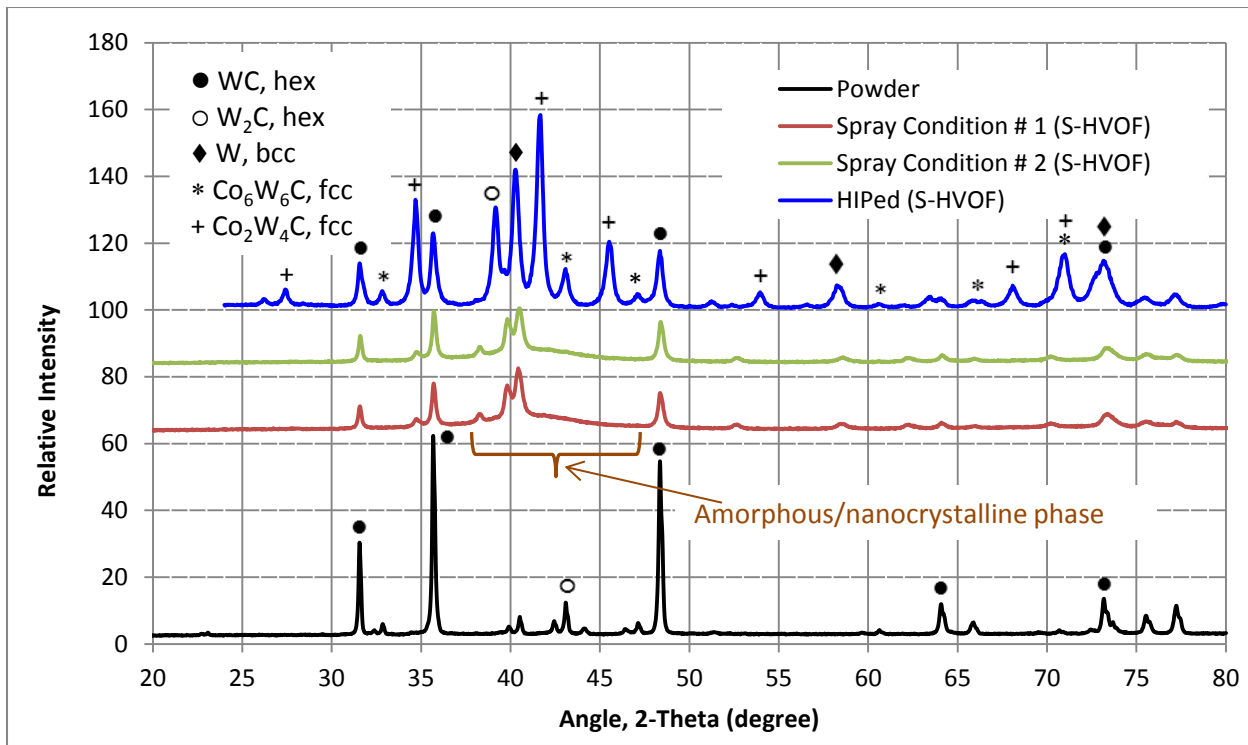


Figure 5, XRD plots of the S-HVOF powder, coating in the as-sprayed and the HIPed conditions

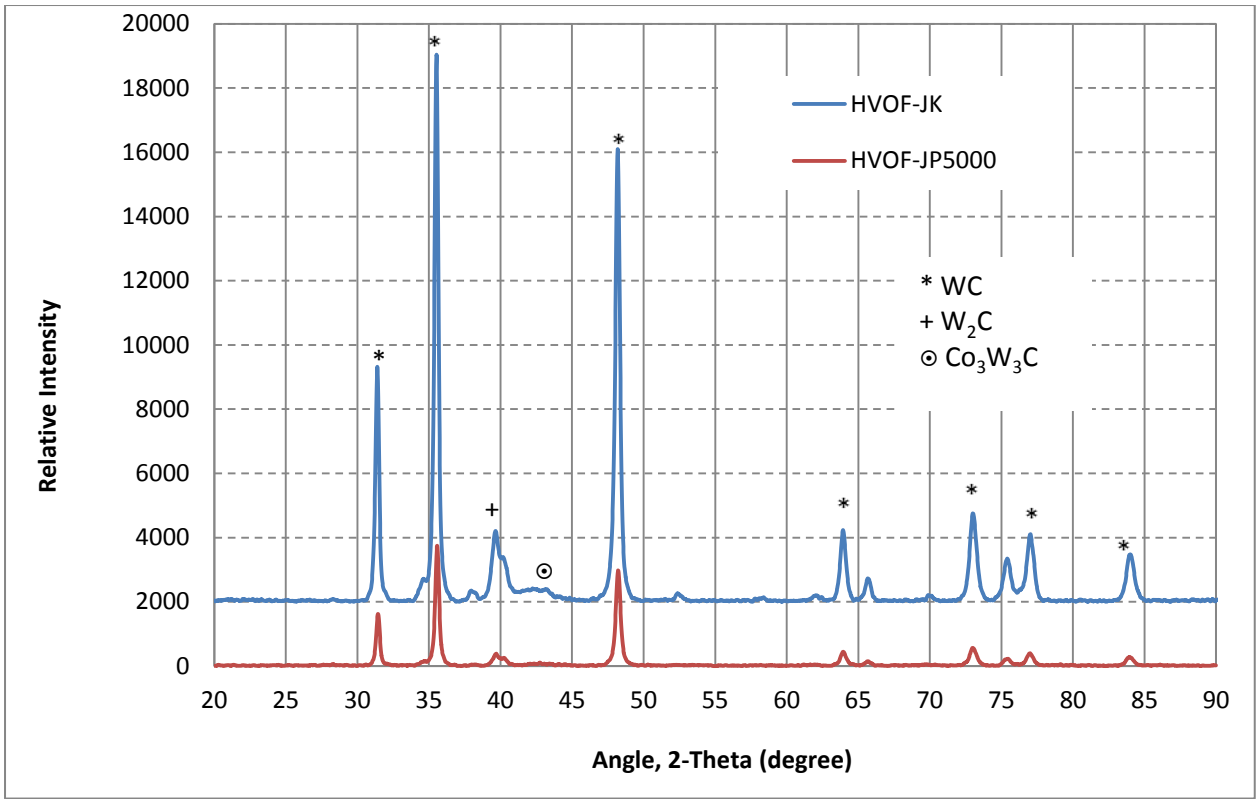
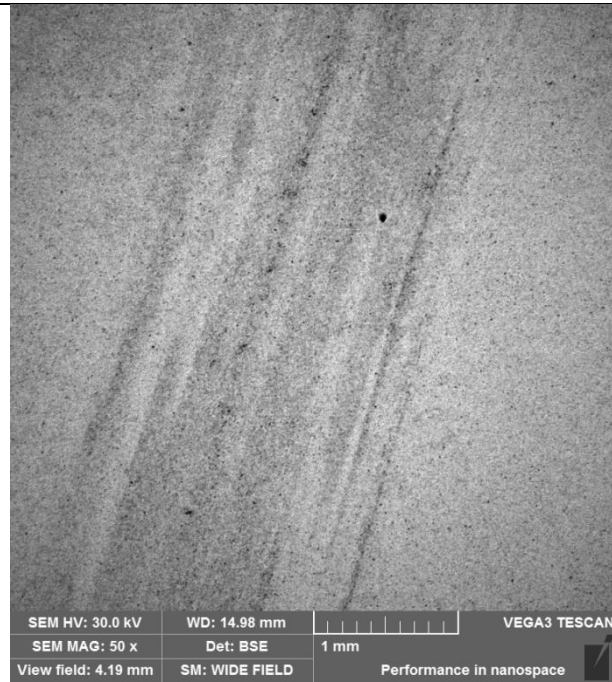
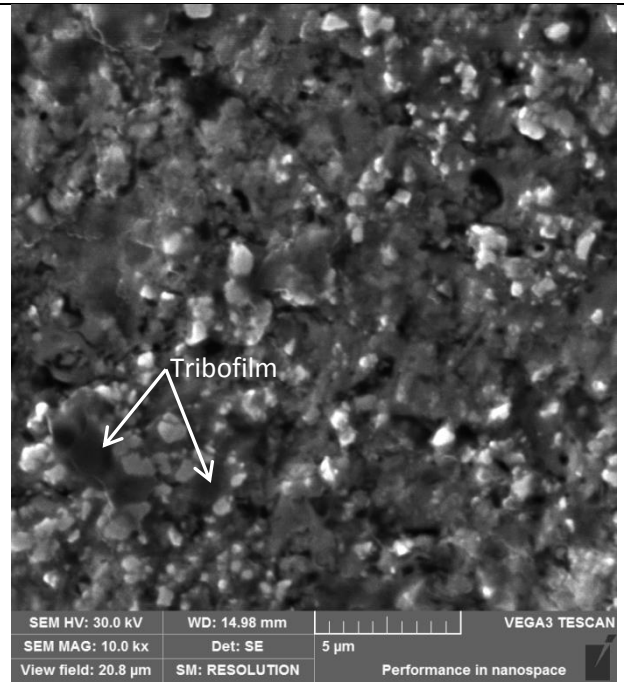


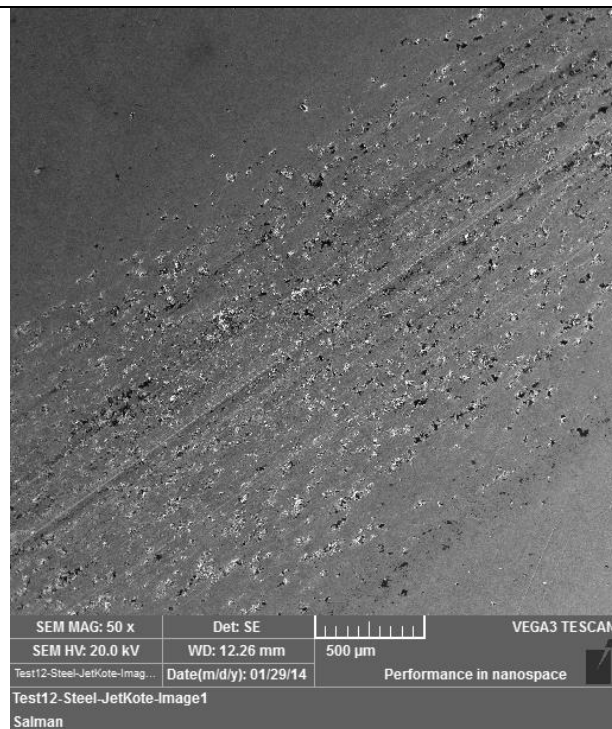
Figure 6, XRD plots of the HVOF-JK and HVOF-JP coatings



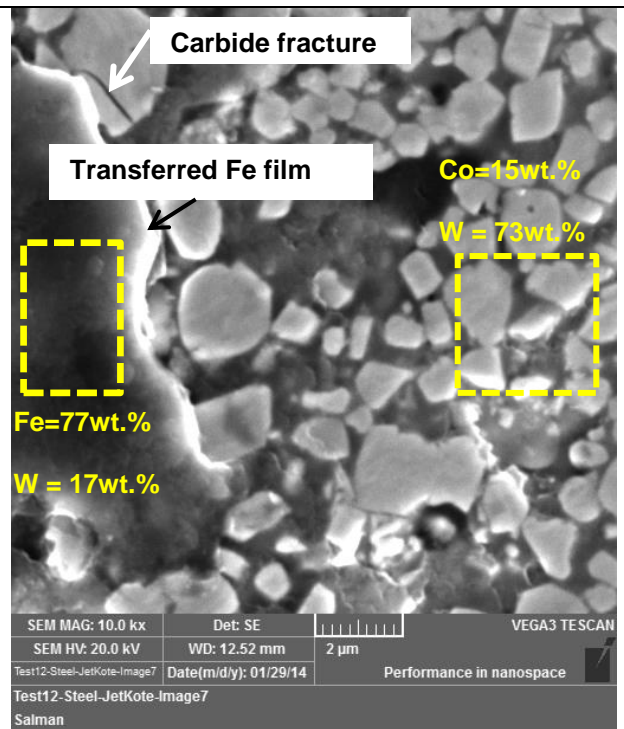
a) S-HVOF



b) S-HVOF



c) HVOF-JK



d) HVOF-JK with EDX results of boxed areas

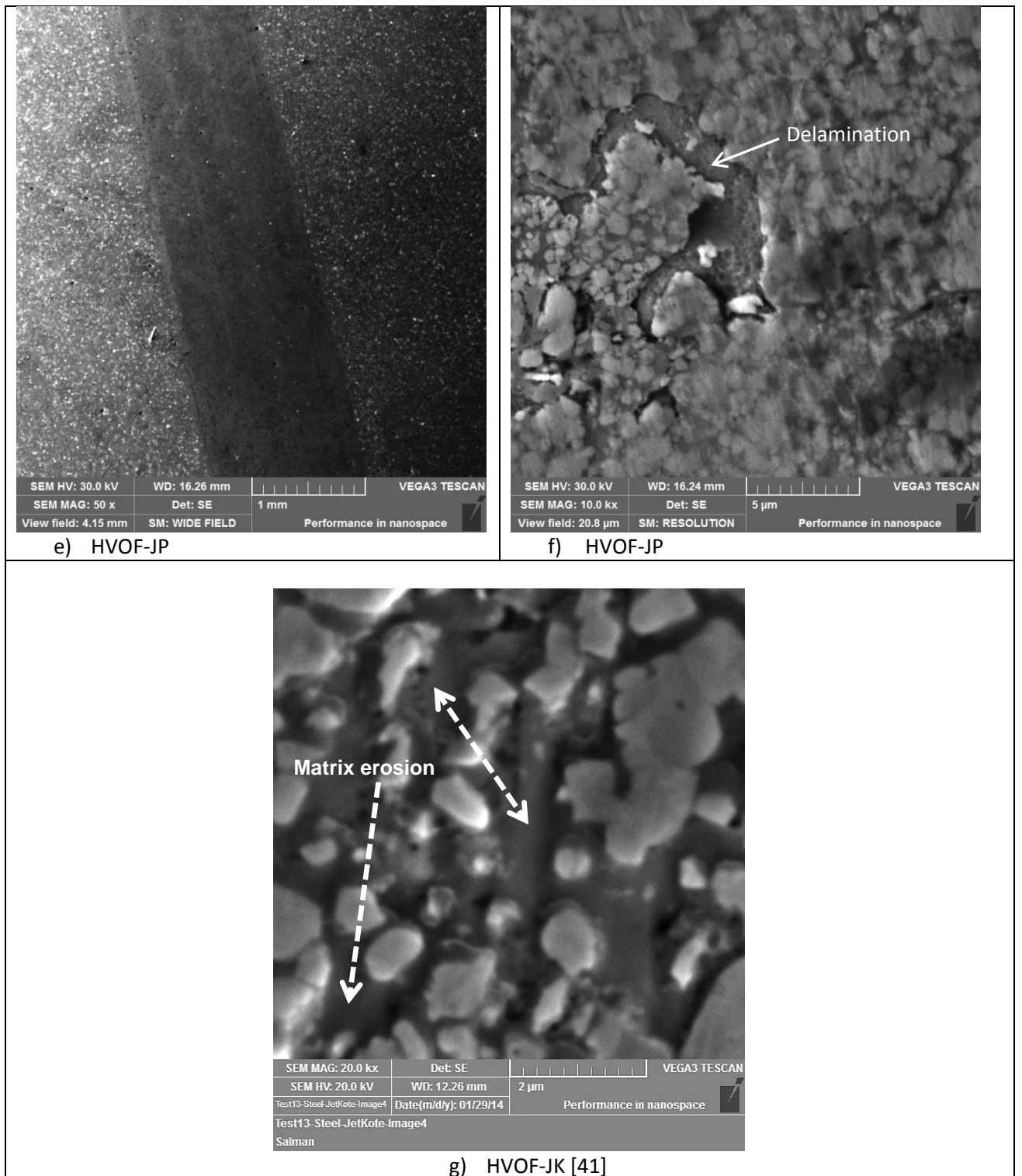
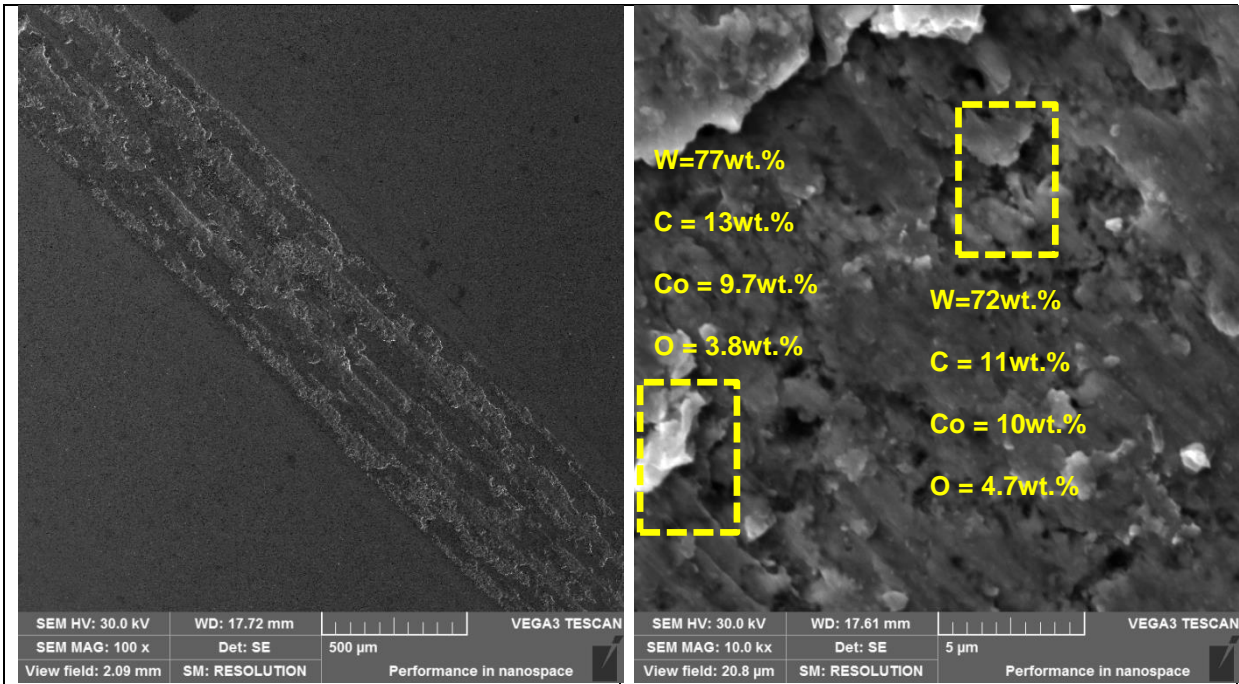
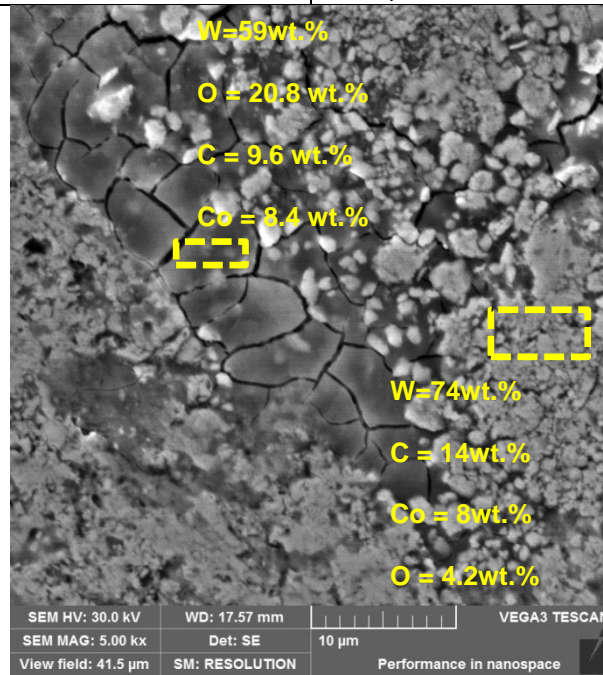


Figure7, Wear track observations of the HVOF coatings against the steel ball

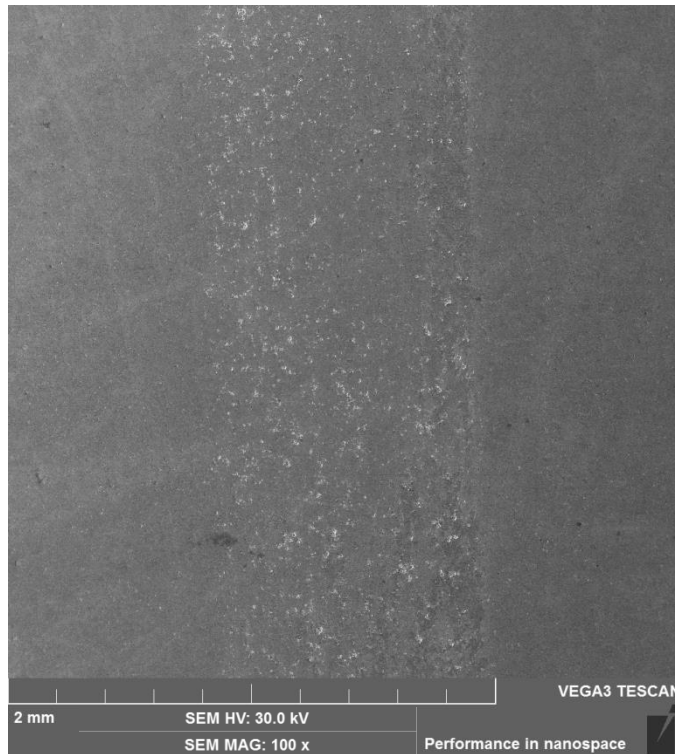


a) S-HVOF

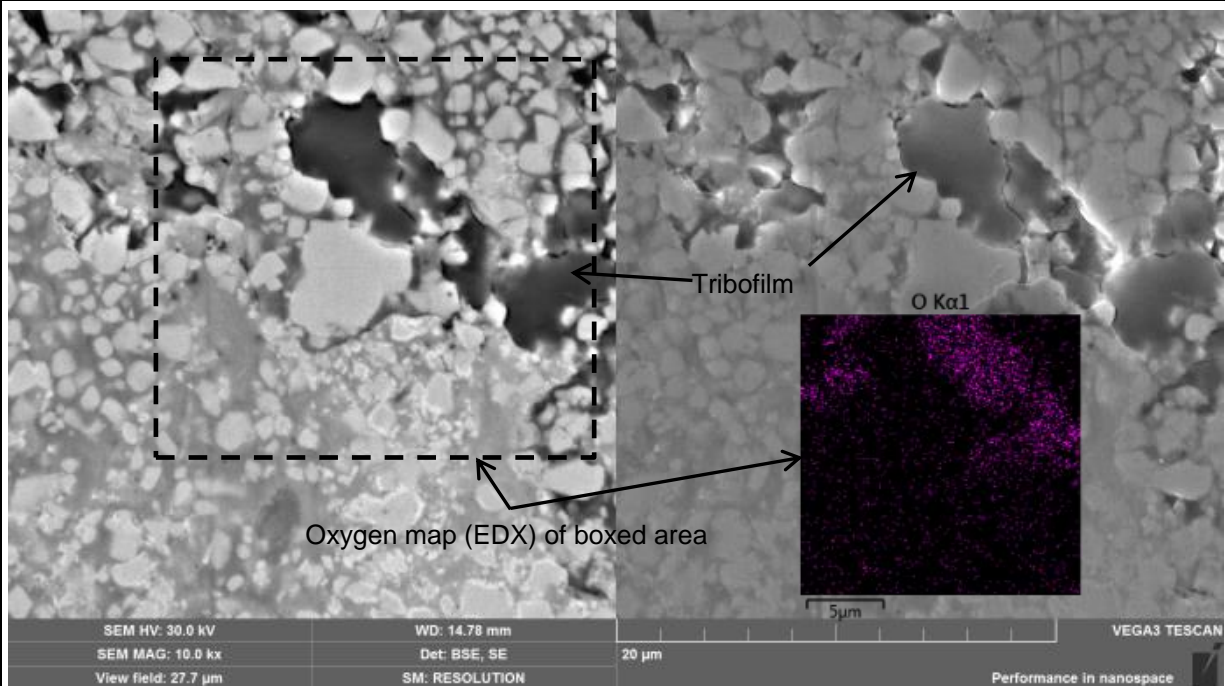
b) S-HVOF with EDX results of boxed areas



c) S-HVOF with EDX results of boxed areas



d) HVOF-JK



e) HVOF-JK with EDX map of oxygen

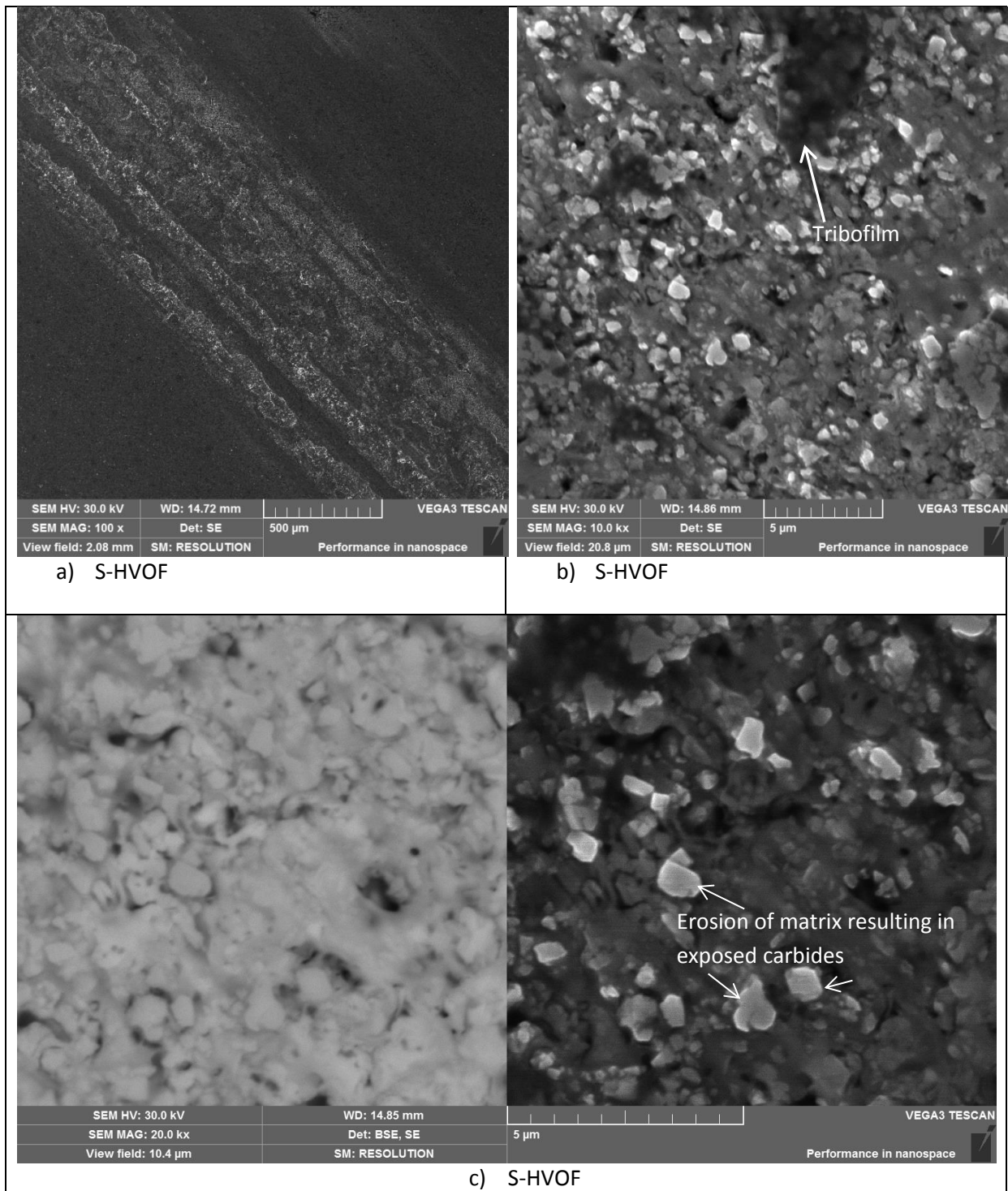
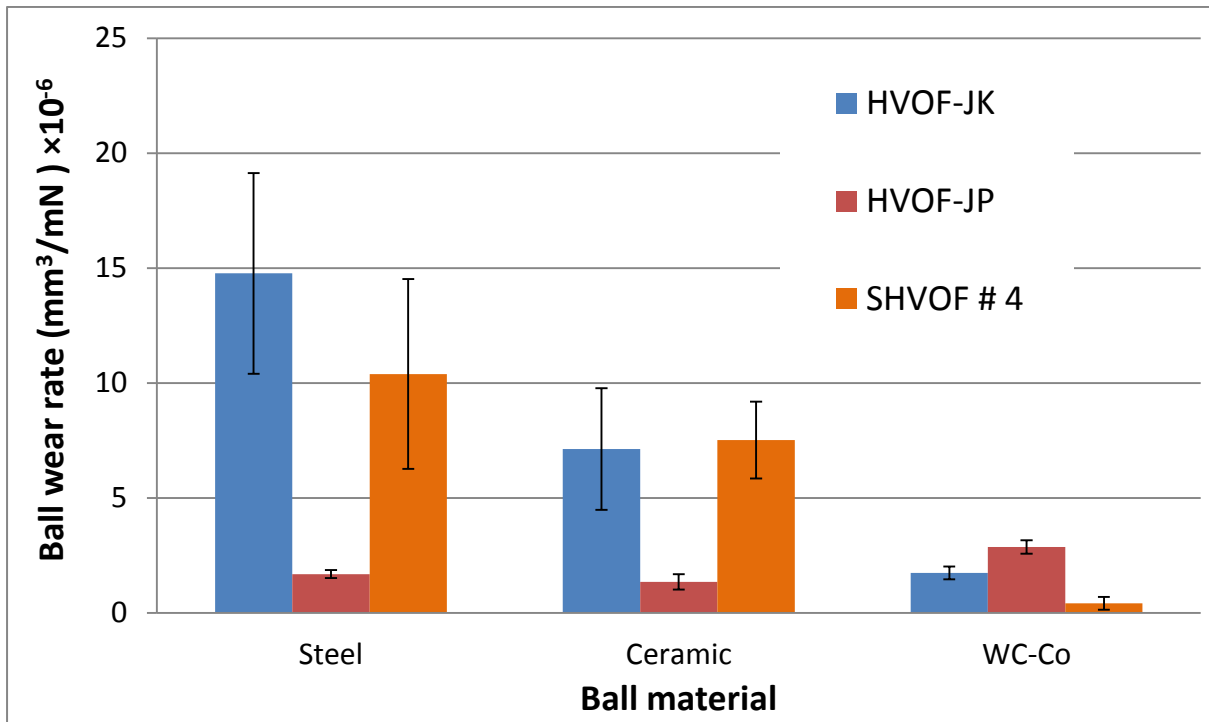
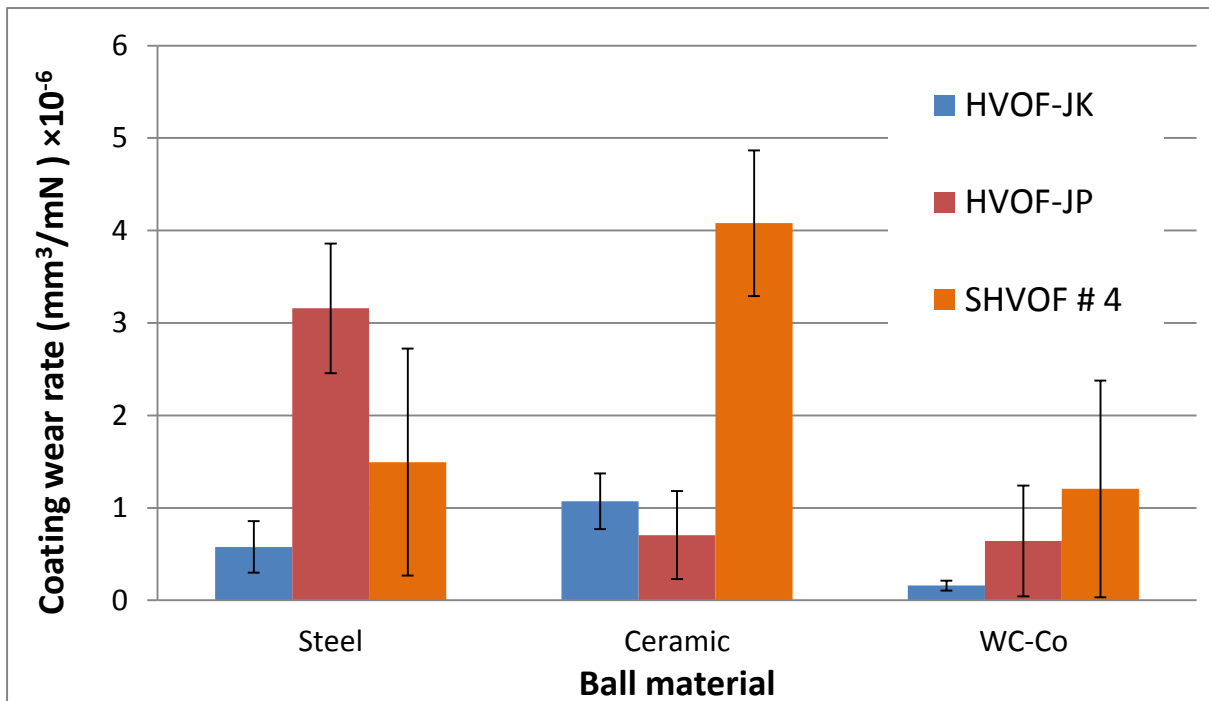


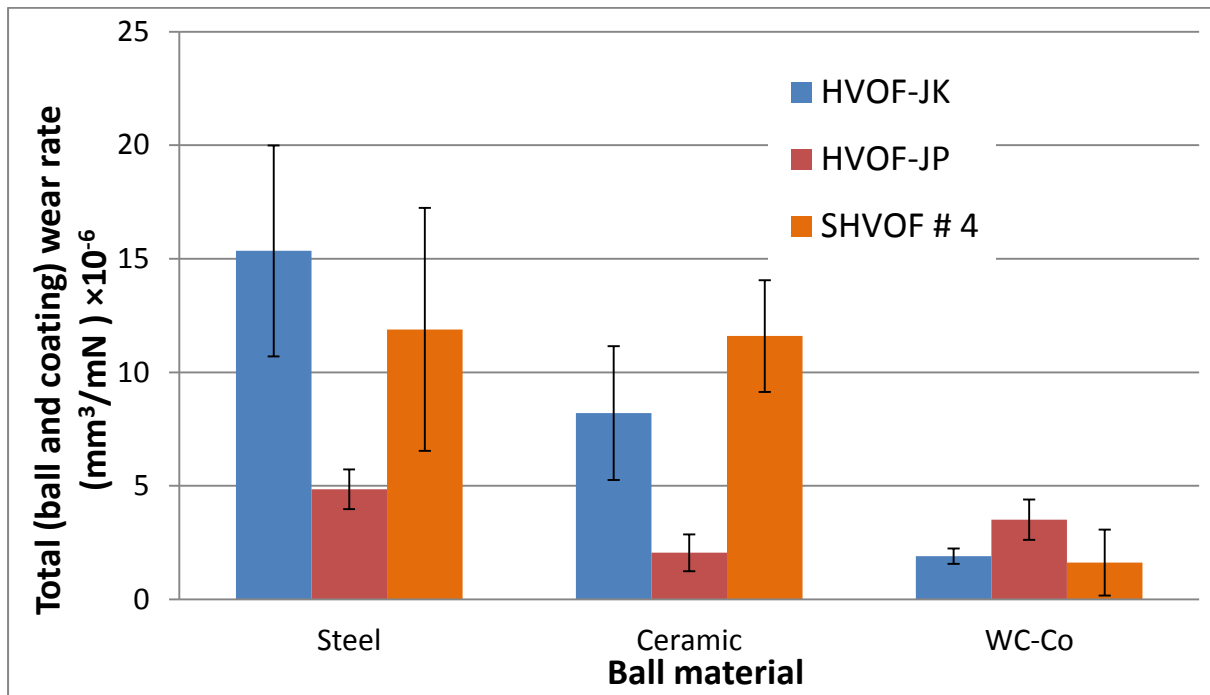
Figure 9, Wear track observations of the HVOF coatings against Si₃N₄ ceramic ball



a, Ball wear rate for the HVOF coatings



b, Coating wear rate against the steel, ceramic (Si_3N_4) and WC-Co balls



c, Total (ball and coating) wear rate against the steel, ceramic (Si_3N_4) and WC-Co balls

Figure 10, Ball, coating and total (ball and coating) wear rates for the S-HVOF (deposition condition # 4), HVOF-JK and HVOF-JP coatings sliding against the steel, Si_3N_4 ceramic and WC-Co balls

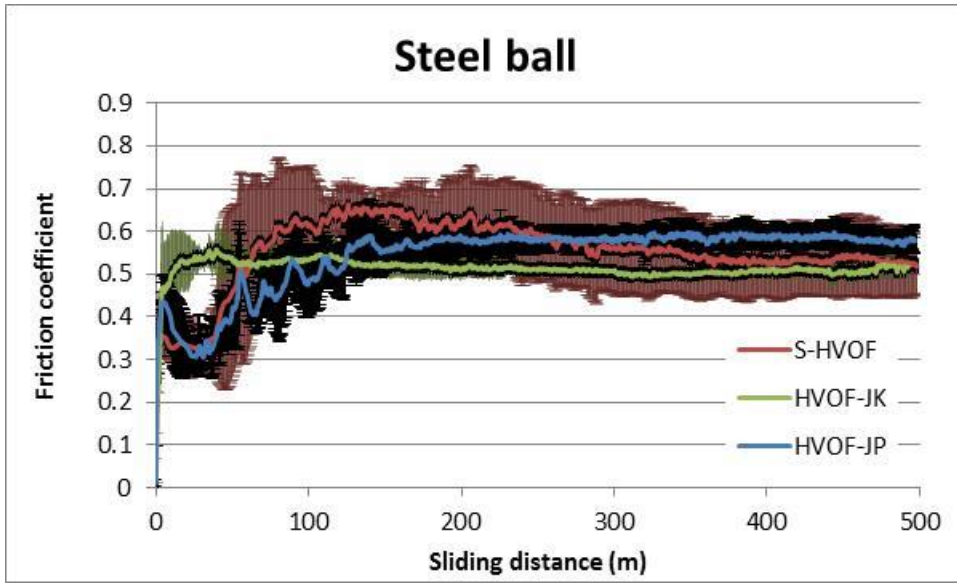


Figure 11(a), Friction coefficient for the steel balls against the S-HVOF and HVOF-JK coating test couples

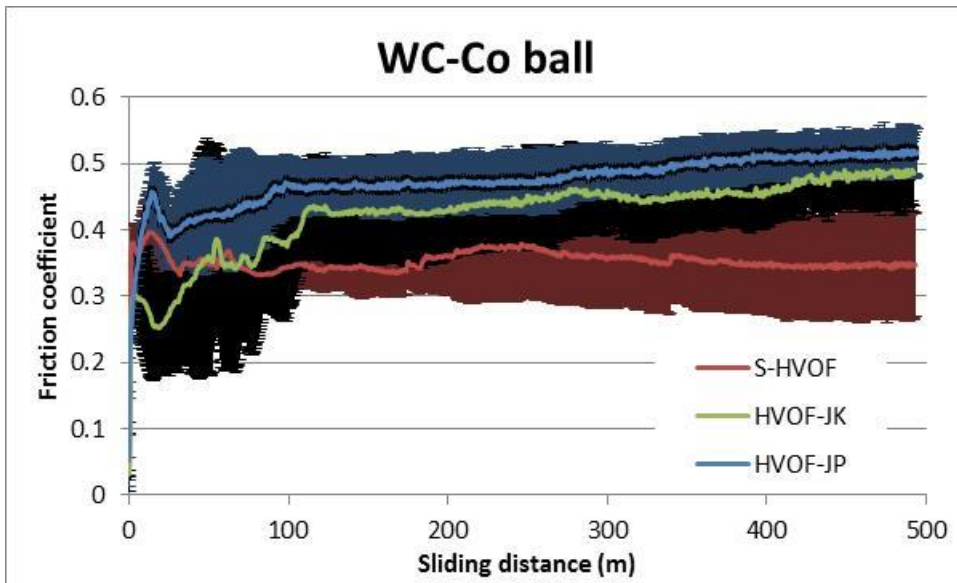


Figure 11(b), Friction coefficient for the WC-Co balls against the S-HVOF and HVOF-JP coating test couples

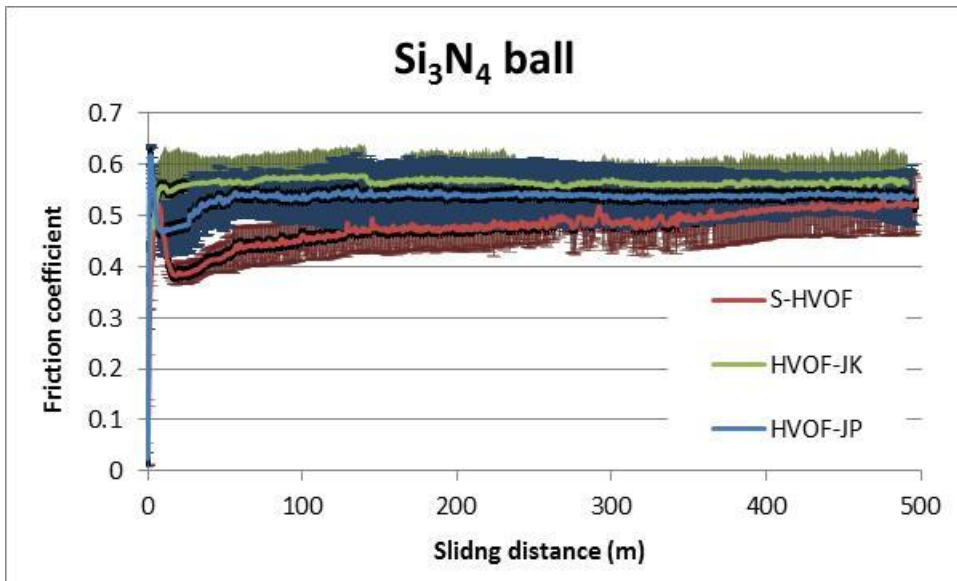
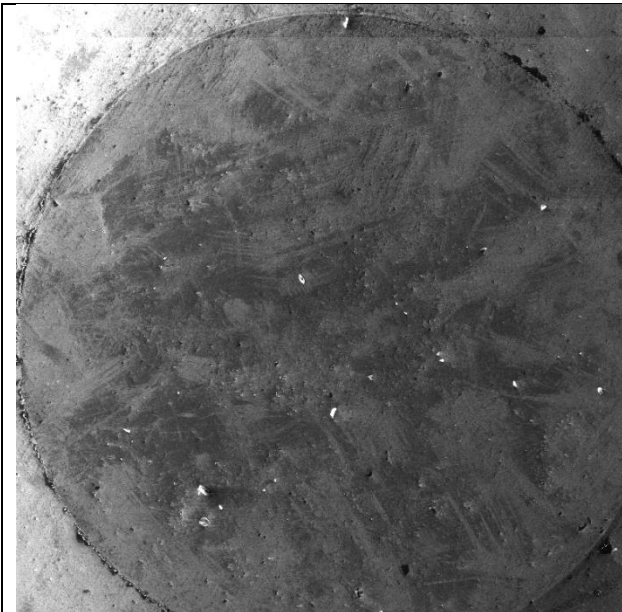
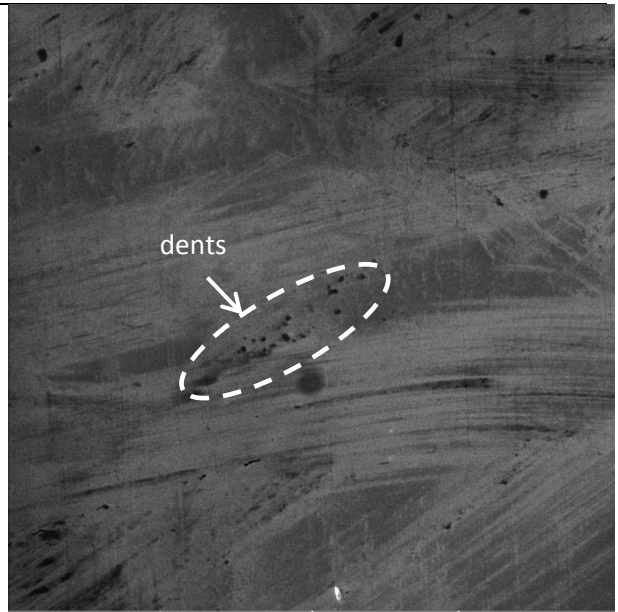


Figure 11(c), Friction coefficient for the Si₃N₄ ceramic balls against the S-HVOF, HVOF-JK and HVOF-JP coating test couples



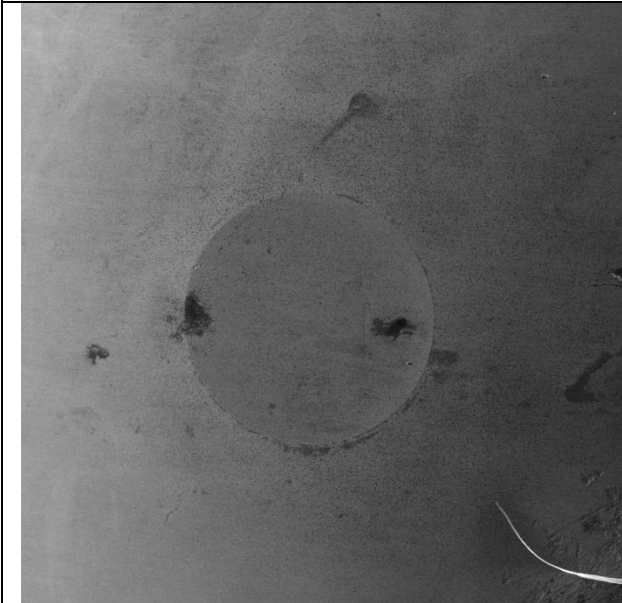
SEM HV: 30.0 kV	WD: 13.00 mm	VEGA3 TESCAN
SEM MAG: 100 x	Det: SE	500 μm
View field: 2.08 mm	SM: RESOLUTION	Performance in nanospace

a) Steel ball



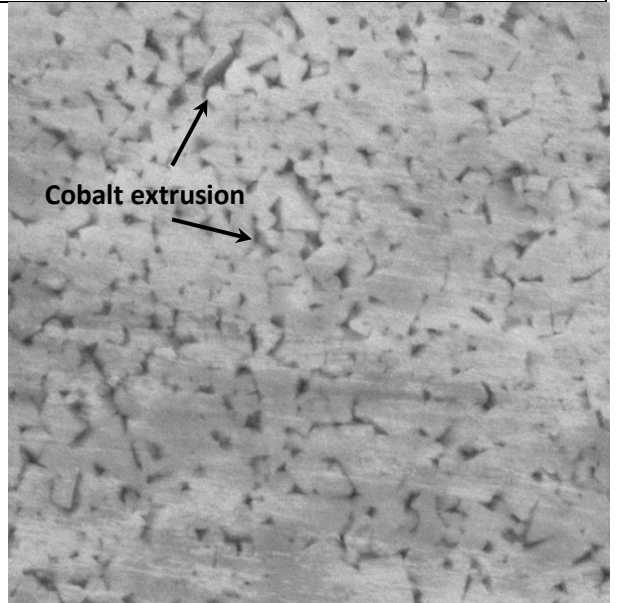
SEM HV: 30.0 kV	WD: 15.41 mm	VEGA3 TESCAN
SEM MAG: 500 x	Det: SE	100 μm
View field: 415 μm	SM: RESOLUTION	Performance in nanospace

b) Steel ball – higher magnification



SEM HV: 30.0 kV	WD: 16.08 mm	VEGA3 TESCAN
SEM MAG: 100 x	Det: SE	500 μm
View field: 2.08 mm	SM: RESOLUTION	Performance in nanospace

c) WC-Co ball



SEM HV: 30.0 kV	WD: 15.00 mm	VEGA3 TESCAN
SEM MAG: 10.00 kx	Det: SE	5 μm
View field: 20.8 μm	SM: RESOLUTION	Performance in nanospace

d) WC-Co ball – higher magnification

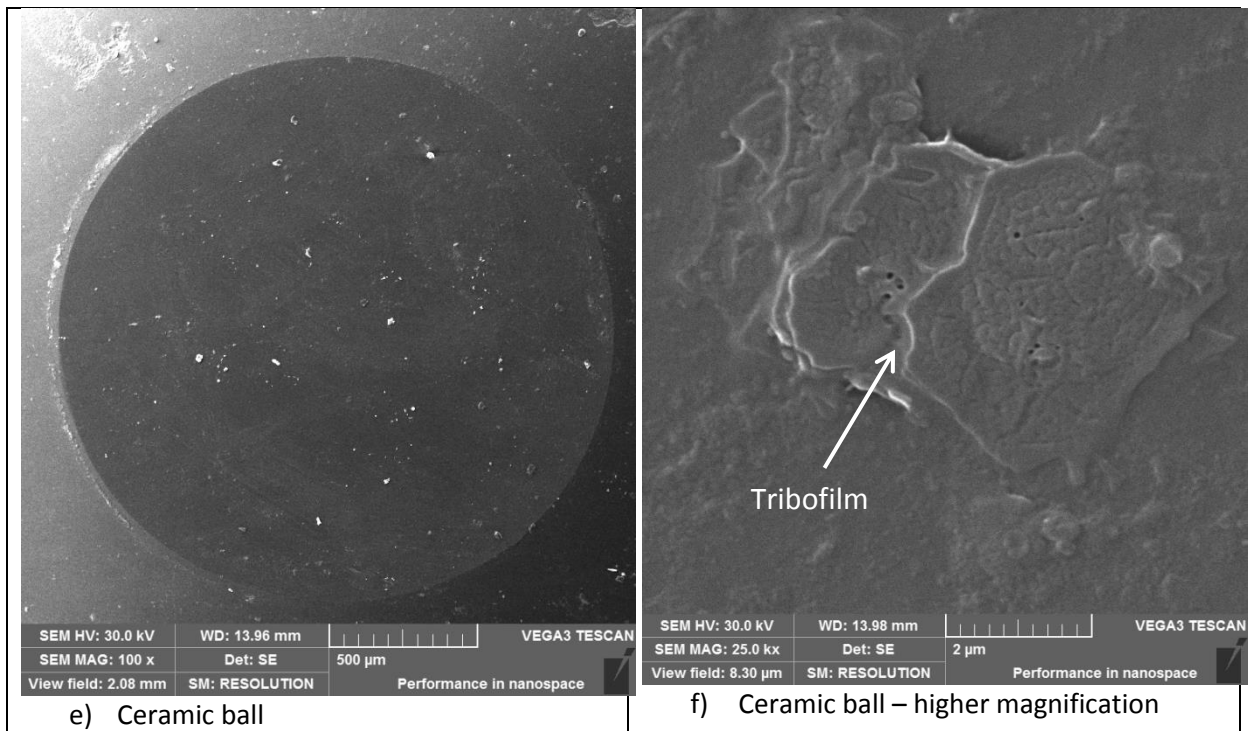


Figure 12, SEM observations of the ball wear scar surfaces for the S-HVOF coatings

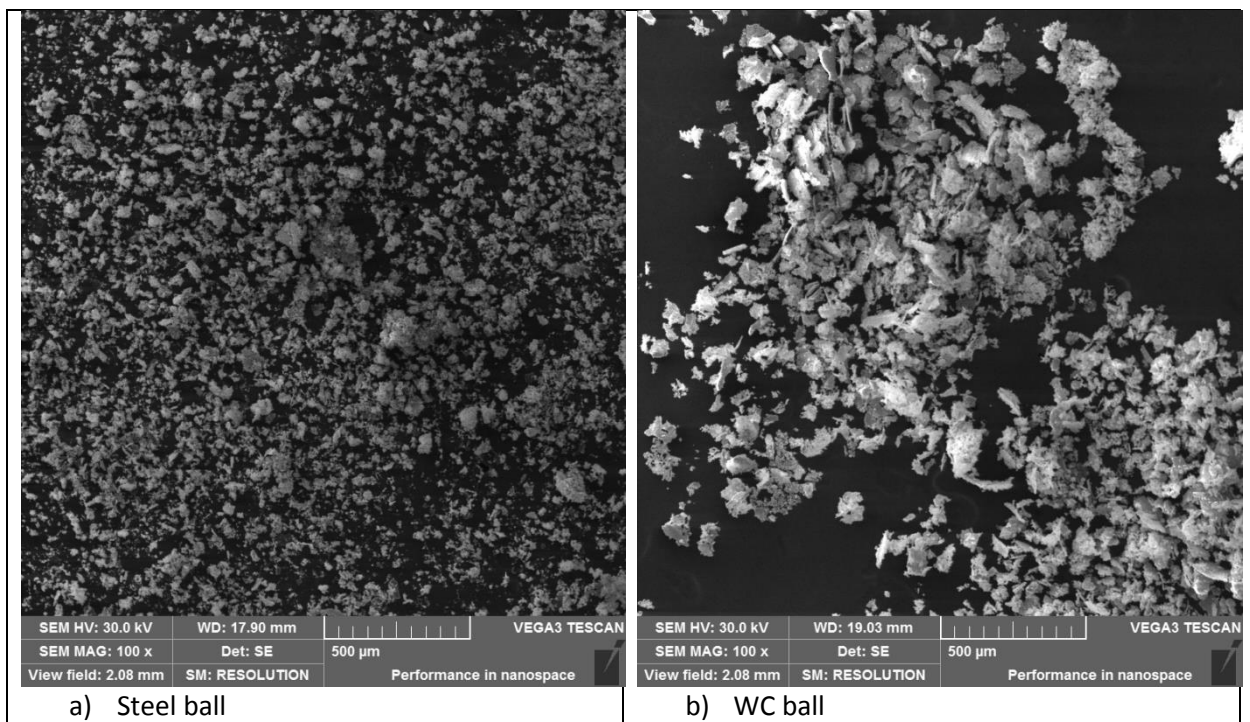
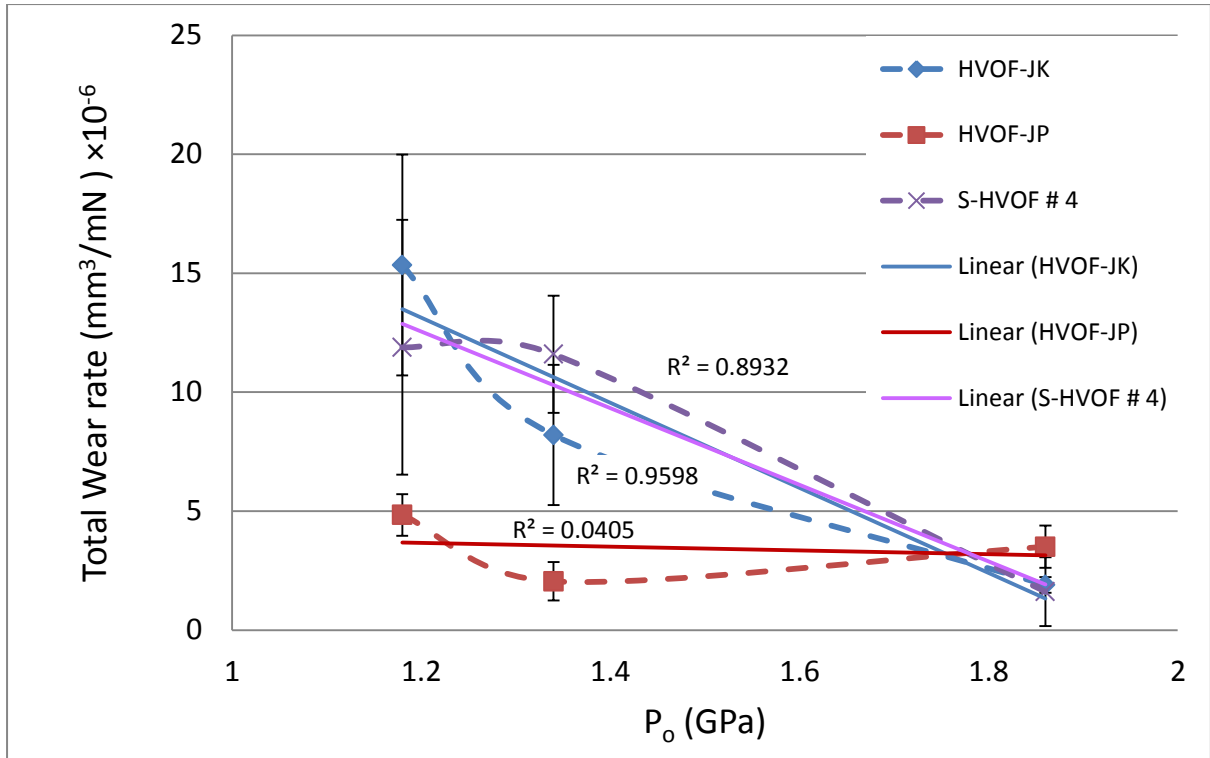
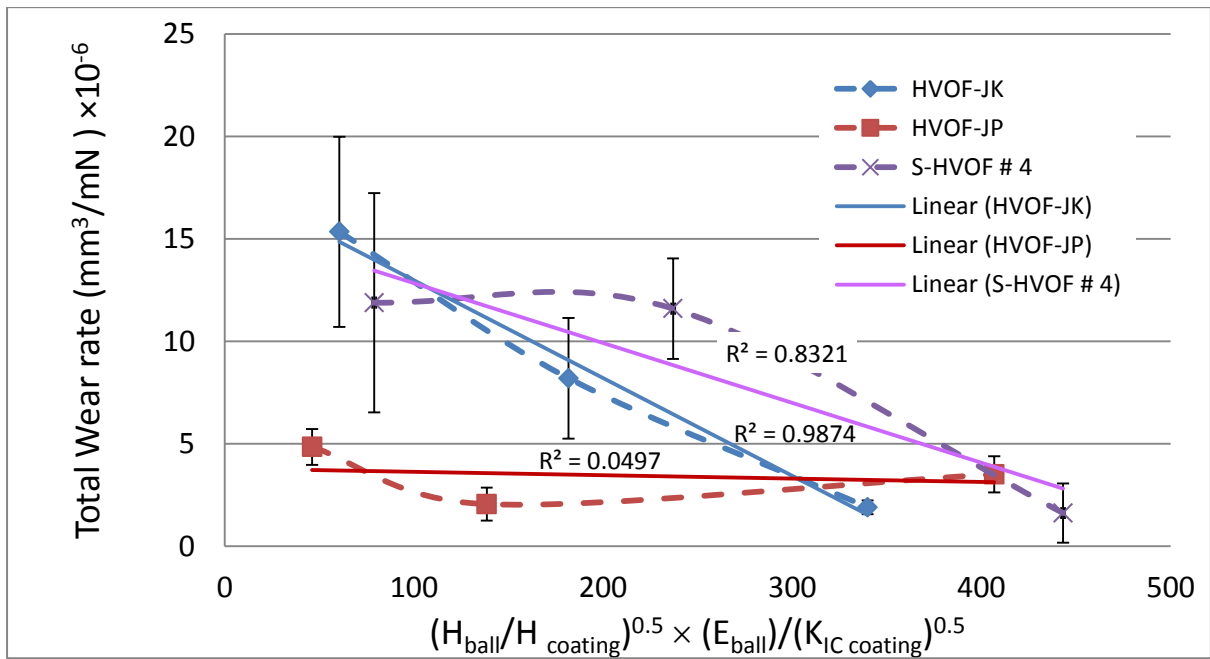


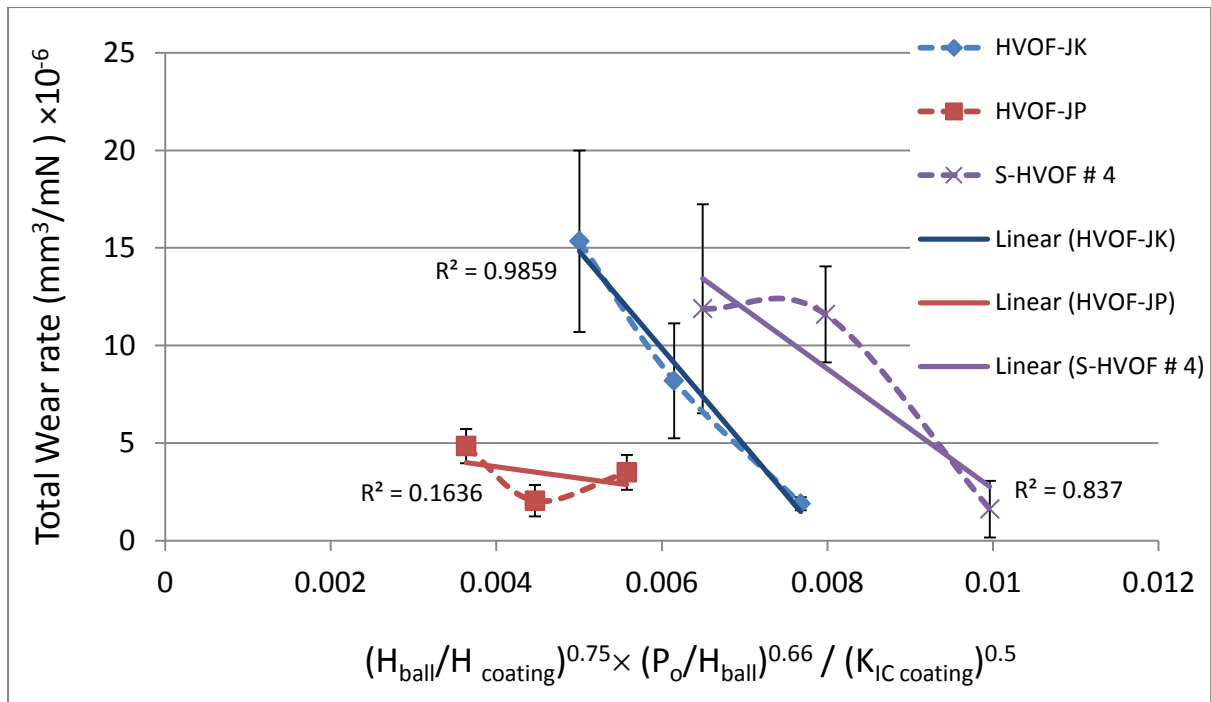
Figure 13, SEM observations of the wear debris for the S-HVOF coatings



a), Total wear rate vs Hertzian contact stress (P_o) at the start of the test



b), Total wear rate vs $\sqrt{\frac{H_{ball}}{H_{coating}}} \times \frac{E_{ball}}{\sqrt{K_{IC\ coating}}}$



c), Total wear rate vs $\left(\frac{H_{\text{ball}}}{H_{\text{coating}}}\right)^{3/4} \times \left(\frac{P_o}{H_{\text{ball}}}\right)^{2/3} / \sqrt{K_{\text{IC coating}}}$

Figure 14, Total wear rate vs the mechanical properties of the ball and coating materials